CORONAVIRUS

A SARS-CoV-2 and influenza double hit vaccine based on RBD-conjugated inactivated influenza A virus

Zhenzhen Wang[1,2], Zhenhua Li[1,2], Weiwei Shi[1,2], Dashuai Zhu[1,2], Shiqi Hu[1,2], Phuong-Uyen C. Dinh[1,2], Ke Cheng[1,2,3]*

The circulating flu viruses merging with the ongoing COVID-19 pandemic raises a more severe threat that promotes the infectivity of SARS-CoV-2 associated with higher mortality rates. Here, we conjugated recombinant receptor binding domain (RBD) of SARS-CoV-2 spike protein onto inactivated influenza A virus (Flu) to develop a SARS-CoV-2 virus-like particle (VLP) vaccine with two-hit protection. This double-hit vaccine (Flu-RBD) not only induced protective immunities against SARS-CoV-2 but also remained functional as a flu vaccine. The Flu core improved the retention and distribution of Flu-RBD vaccine in the draining lymph nodes, with enhanced immunogenicity. In a hamster model of live SARS-CoV-2 infection, two doses of Flu-RBD efficiently protected animals against viral infection. Furthermore, Flu-RBD VLP elicited a strong neutralization activity against both SARS-CoV-2 Delta pseudovirus and wild-type influenza A H1N1 inactivated virus in mice. Overall, the Flu-RBD VLP vaccine is a promising candidate for combating COVID-19, influenza A, and coinfection.

INTRODUCTION

Coronavirus disease 2019 (COVID-19) pandemic, caused by severe acute respiratory syndrome coronavirus 2 (SARS-CoV-2), has led to more than 765 million reported cases and 6.9 million deaths declared by the World Health Organization as of 12 May 2023 (https://covid19.who.int/), severely disrupting public health and social and economic infrastructures (*1*, *2*). Apart from the new coronavirus, seasonal influenza causes sustained epidemics in most nontropical countries and approximately leads to 650,000 deaths every year (*3*). Of special note, SARS-CoV-2 and influenza viruses share similarities clinical manifestations of the respiratory syndrome, common transmission mechanism, the same infection tissues, and seasonal coincidence (*4*–*6*). Recent clinical reports revealed concurrent infections with influenza A virus in 22.3% of cases who died of SARS-CoV-2 and in 19.3% of living patients in Northeastern lran (*7*). In addition, pre-infection with influenza A virus substantially strengthens the entry of SARS-CoV-2 into host cells, resulting in more severe lung damage and a higher mortality rate (*8*). Coinfection of SARS-CoV-2 and flu resulted in 43.1% of dead cases, which SARS-CoV-2 infection alone led to 26.9% of dead cases (*9*). Given that the concomitant circulation infections of SARS-CoV-2 with influenza virus, urgency in the development of an available and viable vaccine capable of controlling both kinds of pandemics and preventing next wave pandemic is of vital important.

SARS-CoV-2 is a single-stranded RNA virus that encodes membrane (M), envelope (E), nucleocapsid (N), and surface spike (S) proteins (*10*). S protein initiates viral entry through its receptor binding domain (RBD) to engage the host cell receptor, angiotensin-converting enzyme 2 (ACE2) (*11*). Recent reports have described that more than 90% of neutralizing humoral responses against SARS-CoV-2 are accountable for RBD-directed antibodies (Abs) (*12*–*14*). Furthermore, it has been proved that RBD is the predominant target of neutralizing Abs of COVID-19 convalescent plasma, which has been used for rescuing mortality in severe cases (*15*, *16*). The relationship between RBD-directed Abs and neutralization capability of COVID-19 patient plasma motivates using RBD as a subunit vaccine immunogen for stimulation of a more focused immune response targeting well-conserved domains (*17*). To date, multiple SARS-CoV-2 vaccines have been developed, of which live attenuated vaccines are particularly attractive as they activate all branches of the host immune system. However, preexisting cross-reactive immunity originated from natural contact with other human coronaviruses might potentially restrict their protective activity against SARS-CoV-2 (*18*). Moreover, live attenuated vaccines have the potential to revert to a wild-type phenotype causing severe diseases. Compared with live-attenuated virus or some viral vectored vaccines, RBD subunit vaccine could eliminate the concerns of preexisting immunity, virulence recovery, and incomplete inactivation due to specific viral antigenic fragments excluding any components of infectious viruses (*19*). Nevertheless, RBD subunit vaccine would necessitate a potent adjuvant or multiple doses to elicit adequate immunogenicity mainly arising from their relatively low immunogenicity due to rapid degradation and clearance (*20*).

Influenza pandemics occur when a strain of influenza virus that has a viral surface protein hemagglutinin (HA), to which there is little or no existing immunity, transmits from human to human within the population (*21*). Among them, pandemic influenza A H1N1 virus circulates in humans and causes annual epidemics around the world since first emerged in April 2009 (*22*). Administration of influenza A vaccine is one effective strategy to prevent infections and severe illnesses. Both live attenuated influenza vaccine and inactivated influenza vaccine were widely used for the public against influenza pandemics. Studies have shown that live attenuated influenza vaccine can reduce the rate of infection as much as 94% and have a higher immunogenicity ability compared to inactivated influenza vaccine (*23*). However, live-attenuated viruses have

[1]Department of Molecular Biomedical Sciences, North Carolina State University, Raleigh, NC 27607, USA. [2]Joint Department of Biomedical Engineering, University of North Carolina at Chapel Hill, Chapel Hill, North Carolina 27599, and North Carolina State University, Raleigh, NC 27606, USA. [3]Division of Pharmacoengineering and Molecular Pharmaceutics, University of North Carolina at Chapel Hill, Chapel Hill, NC 27599, USA.
*Corresponding author. Email: ke_cheng@ncsu.edu, ke_cheng@unc.edu

potential safety concerns, such as increased risks of asthma or wheezing (*24*). Comparatively, inactivated influenza A virus vaccine exhibited a good safety and intrinsic immunogenicity that provides efficient protection for the individual and moderates the impact of an outbreak of influenza on the community (*25*). In particular, clinical analysis indicated that COVID-19 patients who inoculated with influenza A virus vaccine in 2020, even if received after the onset of SARS-CoV-2 infection-related symptoms, had a higher chance of survival and had less need of hospital care than those patients without receiving influenza vaccination (*26*, *27*).

Inspired by both the outstanding characteristics of inactivated influenza A virus and RBD, we conjugated RBD onto the surface of inactivated influenza A virus, creating a SARS-CoV-2 virus-like particle (VLP) vaccine with potential two-hit protective activity that not only induced the generation of RBD-specific immunoglobulin G (IgG) antibody but also produced HA antigen-specific antibody responses (Fig. 1). Here, inactivated influenza A (H1N1) virus (Flu) was used to conjugate with RBD (designated as Flu-RBD). We demonstrated that Flu could serve as a safe and flexible platform to improve the retention of RBD in draining lymph nodes (LNs) and trigger a stronger humoral and cellular immunity relative to free RBD and the mixture of unconjugated RBD with Flu. This strengthened the functional immunogenicity of RBD antigen. We tested this vaccine using a hamster model of live SARS-CoV-2 challenge, where two doses of Flu-RBD vaccination were verified to be safe and efficacious, providing protective activities against SARS-CoV-2 infection. Furthermore, we demonstrated that Flu-RBD vaccinations exhibited substantial neutralization ability against SARS-CoV-2 Delta pseudovirus variants and wild-type influenza A H1N1 inactivated virus in mice.

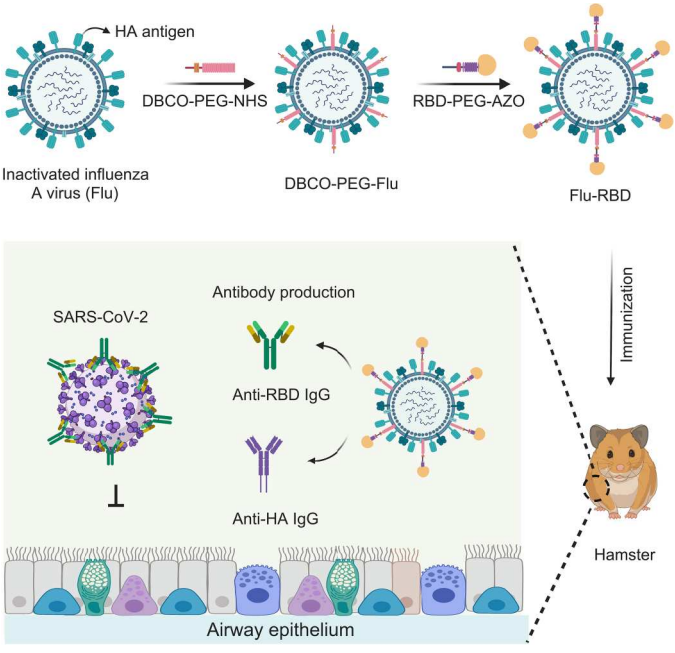

Fig. 1. Flu-RBD VLP vaccine induces the neutralization of SARS-CoV-2 in hamsters. Flu-RBD functions as a two-hit vaccine, eliciting both RBD-specific and HA-specific IgG antibody responses against SARS-CoV-2 infection in hamsters.

RESULTS

Fabrication and characterization of Flu-RBD VLP vaccine

To construct the Flu-RBD VLP vaccine, RBD antigen was modified with azido–polyethylene glycol–*N*-hydroxysuccinimidyl ester (AZO-PEG-NHS). SDS–polyacrylamide gel electrophoresis revealed the successfully conjugation of RBD with AZO-PEG-NHS (RBD-PEG-AZO) who ran more slowly than free RBD (fig. S1). Fourier transform infrared spectroscopy (FTIR) analysis further demonstrated that the successfully preparation of RBD-PEG-AZO as indicated by the presence of -N≡N stretching vibration located at 2161 cm^{-1} (fig. S2). Meanwhile, Flu was conjugated with dibenzocyclooctyne (DBCO)-PEG-NHS to synthesize DBCO-PEG-Flu, which demonstrated by the FTIR analysis (fig. S3). Through the bio-orthogonal click reaction of DBCO with AZO, RBD was anchored on the surface of Flu successfully; in this way, a Flu-RBD vaccine with double-protecting ability was fabricated (Fig. 2A). Immunoblotting analysis showed that RBD band was presented in Flu-RBD and RBD lysates rather than in Flu lysate (Fig. 2B). Likewise, HA band, the marker of Flu, was observed in both Flu-RBD and Flu lysates but in free RBD (Fig. 2B). In addition, distinct immunogold nanoparticles against RBD antigen were found on the surface of Flu (Fig. 2C), indicative of the conjugation of RBD with Flu. FTIR results further demonstrated the successful preparation of Flu-RBD (fig. S3). In addition, we found that RBD modification caused a slight increase in the average diameter of Flu-RBD as evidenced by nanoparticle tracking analysis (NTA) (Fig. 2D). The reaction efficiency of RBD with Flu was calculated to be 71%, indicating that there is 0.71-μg RBD presented per 10^{10} Flu particles. Theoretically, approximately 1669 RBD molecules were bound to each individual Flu. Moreover, this conjugation strategy of RBD on Flu has little effect on the conformation and binding sites of RBD (fig. S4), ensuring its immunogenic profile as an antigen. Collectively, these results confirmed the successful synthesis of Flu-RBD VLP vaccine.

Biodistribution of Flu-RBD vaccine after intramuscular injection

To be effective vaccines, the platform should promote the trafficking of antigen from injection site to draining LNs (*28*). Toward this end, free RBD and Flu-RBD were labeled with Rhodamine (RhB) to evaluate their microscopic distribution in vivo. Both were intramuscularly (i.m.) injected into the right hind limb of mice. The proximal and distal LNs from injection sites, including right and left inguinal LNs as well as cervical LNs, were collected. As illustrated in Fig. 2 (E and F), ex vivo fluorescence imaging and analysis of LNs showed that mice received with Flu-RBD were sacrificed 24 hours postinjection exhibited the greatest integrated density. These proportions in draining LNs at 24 hours after treatment with Flu-RBD were significantly higher than those treated with free RBD. These results suggested that Flu core improves the retention and distribution of RBD in both superficial and cervical LNs. In addition, we moved on to evaluate whether Flu-RBD could be delivered into major organs of animals after i.m. injection. As shown in fig. S5, Flu-RBD-RhB was discovered in the spleen, liver, kidneys, lung, and heart, which in line with the previous report that the intramuscularly injected nanoparticles could be absorbed into the bloodstream quickly (*29*). Compared to Flu-RBD-RhB, lower RBD signals were observed in the mice treated RBD-RhB group due to the rapid clearance of free RBD in vivo.

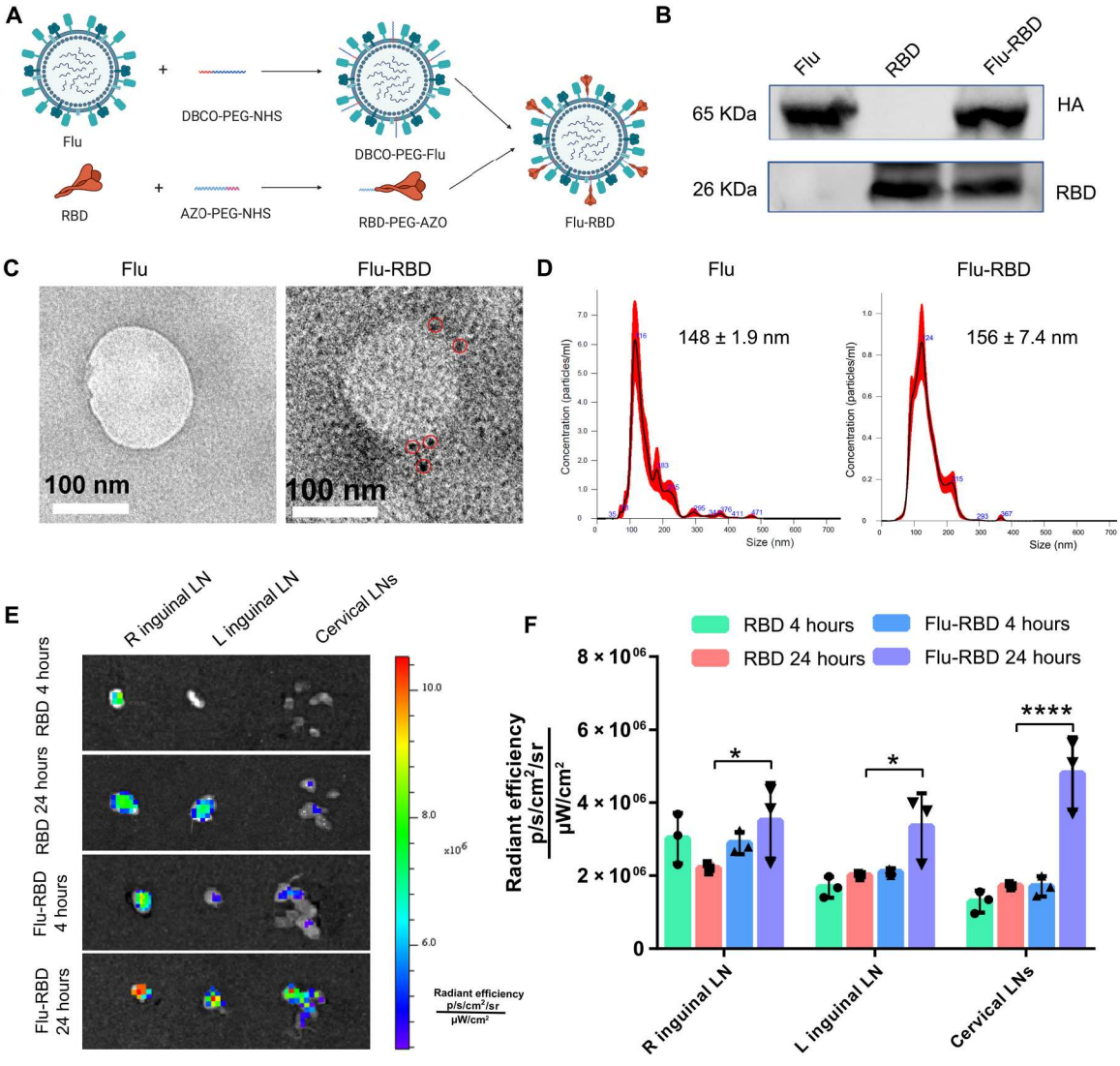

Fig. 2. Characterization of Flu-RBD vaccine and its distribution in draining LNs. (**A**) Schematic displaying the fabrication of Flu-RBD. (**B**) Immunoblots of RBD and HA for Flu, RBD, and Flu-RBD lysates. (**C**) Transmission electron microscopy images of Flu and immune-gold–labeled Flu-RBD. Six nanometers of gold nanoparticles was used to label RBD. (**D**) NTA of Flu and Flu-RBD. (**E**) Ex vivo fluorescence imaging of mouse LNs, including right (R), left (L) inguinal, and cervical LNs, in 4 and 24 hours RBD or Flu-RBD postinjection, where RBD and Flu-RBD were labeled with Rhodamine (RhB) dye, respectively. (**F**) Quantification the integrated density of RhB dye in mice LNs. $n = 3$. Data are mean ± SD. Statistical analysis was performed by two-way analysis of variance (ANOVA) with Tukey's multiple comparisons. *$P < 0.05$; ****$P < 0.0001$. All replicates are biological.

Internalization of Flu-RBD by antigen-presenting cells

Efficient antigen uptake by antigen-presenting cells (APCs) is the key for vaccines to trigger immune response (*19*). Before assessing the internalization of Flu-RBD by APCs, we found that the proportion of Flu-RBD–positive lymphocytes in LNs were significantly higher than those in the LNs treated with free RBD (fig. S6A), indicating that Flu-RBD promoted internalization into LNs. Compared to free RBD, more $CD11c^+$ $F4/80^-$ APCs were found to colocalize with Flu-RBD–positive lymphocytes (fig. S6B). The weighted colocalization coefficient of Flu-RBD with $CD11c^+$ $F4/80^-$ APCs was determined to be 0.37, which decreases to 0.24 for RBD group (fig. S6, C and D). Furthermore, significantly more $CD11b^+$ APCs were found in the LNs injected with Flu-RBD but free RBD (fig. S7A). Moreover, Flu significantly boosted the uptake of RBD by $CD11b^+$ APCs (fig. S7B). These results suggested that Flu was an efficient platform to overcome the limitations of RBD in vivo and promote the internalization of RBD by APCs, which could be of great interest for improving the functional immunogenicity of RBD.

Humoral immune responses to the Flu-RBD vaccine

CD 1 mice were administered two doses of Flu-RBD at an interval of 1 week, while others immunized with two doses of phosphate-buffered saline (PBS) or Flu or RBD or a mixture of Flu with RBD (Flu-M-RBD) at the same interval (Fig. 3A). As corresponding antibody responses illustrated in Fig. 3B, Flu-RBD elicited the highest level of RBD-specific IgG antibody titer in murine serum. We further evaluated the RBD-specific IgG subclass antibody responses. As shown in Fig. 3C, both free RBD and Flu-M-RBD induced a T helper cell

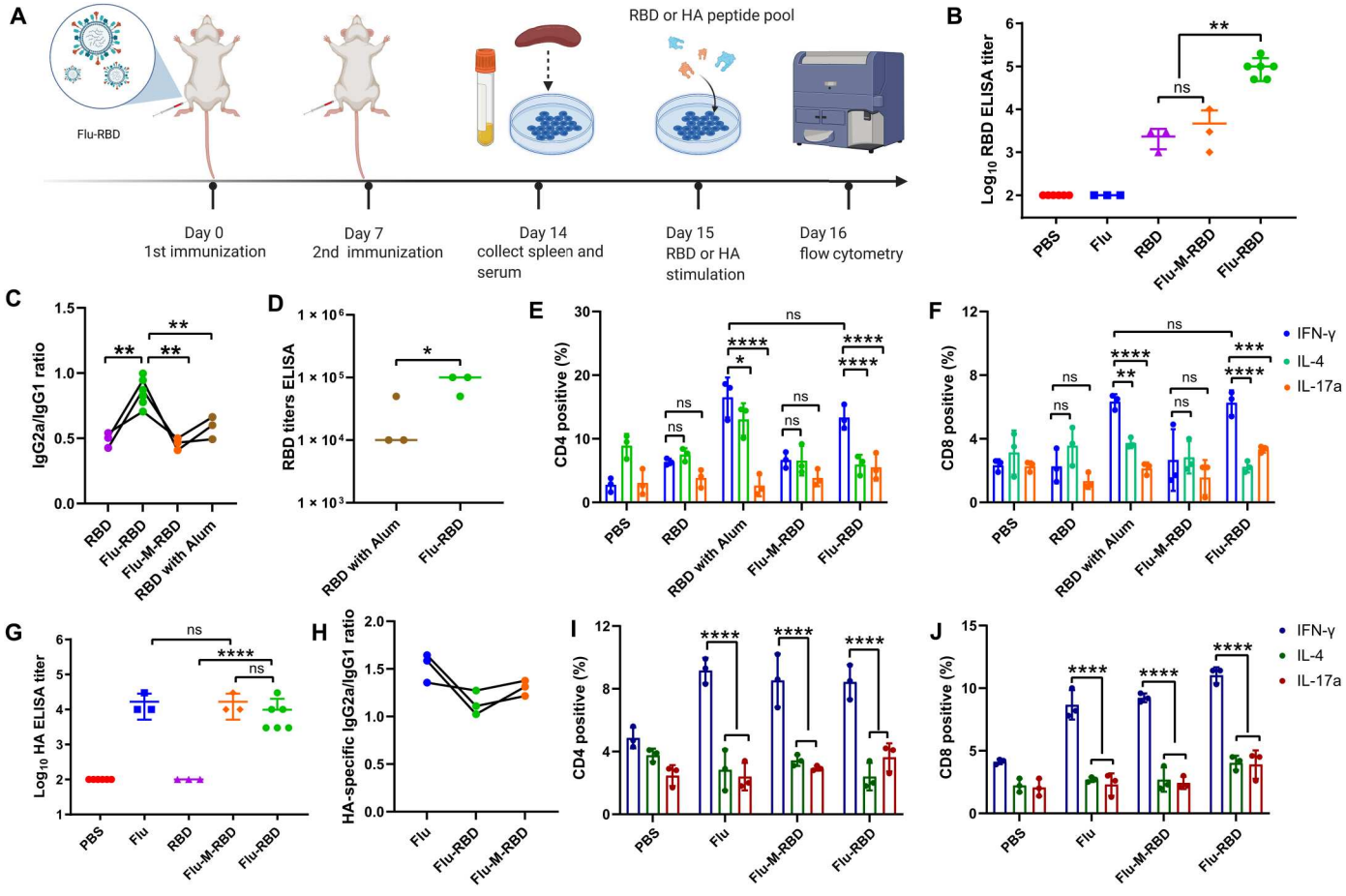

Fig. 3. Humoral immune responses in Flu-RBD–vaccinated mice. (**A**) Schematic illustrating the design of immunizations and sample collections in mice. (**B**) Anti-RBD antibody titers in murine serum determined by ELISA after two vaccinations. $n = 3$ or 6. (**C**) Comparison of ratios of RBD-specific IgG2a and IgG1 from murine serum in different groups, $n = 3$ or 6. (**D**) IgG titers against SARS-CoV-2 RBD in murine serum collected after two immunizations of Flu-RBD or RBD adjuvanted with Alum. $n = 3$. IFN-γ^+ or IL-4$^+$ or IL-17a$^+$ of CD4+ T cells (**E**) and CD8+ T cells (**F**) in the splenocytes in response to RBD peptide pool at week 1 after two vaccinations. $n = 3$. Anti-HA antibody titers (**G**) and the ratio of HA-specific IgG2a and IgG1 (**H**) in murine serum determined by ELISA after two vaccinations. $n = 3$ or 6. IFN-γ^+ or IL-4$^+$ or IL-17a$^+$ of CD4$^+$ T cells (**I**) and CD8$^+$ T cells (**J**) in the splenocytes in response to HA peptide pool at week 1 after two vaccinations. $n = 3$. Each dot represents data from one animal. Data are mean ± SD. Statistical analysis was performed by the two-tailed, unpaired Student's *t* test (B to D, G, and H) or two-way ANOVA tests with a Tukey post hoc test for multiple comparisons (E, F, I, and J). *$P < 0.05$; **$P < 0.01$; ***$P < 0.001$; ****$P < 0.0001$. ns indicates no significance. All replicates are biological.

(T_H2)–biased humoral response as validated by a primary production of IgG1 antibody, whereas Flu-RBD vaccine induced a more balanced T_H1/T_H2-type response with substantially increased levels of IgG2a. Furthermore, Flu-RBD elicited a higher RBD-specific IgG titer than RBD adjuvanted with aluminum (Alum) (Fig. 3D), which could be attributed to enhanced uptake of RBD by APCs. Notably, RBD with Alum induced a T_H2-mediated humoral response as compared with Flu-RBD (Fig. 3C). After restimulation with a RBD peptide pool, SARS-CoV-2–specific CD4$^+$ and CD8$^+$ T cell responses in splenocytes were determined. Compared to RBD or Flu-M-RBD, Flu-RBD triggered a higher population of interferon-γ (IFN-γ) (T_H1) generating CD4$^+$ and CD8$^+$ T cells instead of interleukin-4 (IL-4) (T_H2) or IL-17a (T_H17) generating CD4$^+$ and CD8$^+$ T cells (Fig. 3, E and F). These findings indicated that Flu-RBD elicited T_H1-biased cellular immune responses. In addition, we found that Flu-RBD induced a higher T_H1/T_H2 ratio of produced CD4$^+$ and CD8$^+$ T cells than RBD with Alum (fig. S8). These results are extraordinary as the primary safety consideration when designing SARS-CoV-2 vaccines is inducing a robust T_H1-biased immune response, while avoiding a T_H2-type immune response that may evoke vaccine-associated enhanced respiratory diseases (*30*). Furthermore, we observed that Flu-RBD vaccinations induced a higher frequency of CD4$^+$ and CD8$^+$ T cells expressing IL-17a than free RBD or RBD with Alum vaccinations, indicating that a higher T_H17 immune response was generated (Fig. 3, E and F, and fig. S8).

To compare the immunogenicity of Flu-RBD with the clinical standard mRNA vaccine, we encoded the full-length of spike (S) protein with the same sequence as the Pfizer BNT162b2 (*31*, *32*). According to Pfizer's reports, the prepared mRNA was formulated in lipid nanoparticles to synthesize mRNA-lipid nanoparticles (LNP@mRNA) (*33*, *34*). In addition, commercial Lipofectamine 3000 (Lipo3000) was used to deliver mRNA (Lipo3000@mRNA) as a control. Their cellular translation in vitro was verified by immunoblotting (fig. S9, A and B), where LNP@mRNA showed a higher S protein expression than Lipo3000@mRNA in human embryonic

kidney (HEK) 293 cells. Immunogenicity comparisons of Flu-RBD vaccine with mRNA vaccines in mice were performed. Antibody titers revealed that Flu-RBD induced a higher level of RBD-specific IgG antibody and a higher IgG2a/IgG1 ratio in mouse sera than LNP@mRNA or Lipo3000@mRNA vaccinations (fig. S9, C and D). Flow cytometry results further demonstrated that LNP@mRNA or Lipo3000@mRNA vaccinations were unable to elicit a T_H1-skewing immune response in splenocytes as observed in Flu-RBD vaccinations (fig. S9, E and F). We further assessed the ability of Flu-RBD to clear inhaled SARS-CoV-2 Delta pseudovirus with a red fluorescent protein (RFP) reporter in mice and compared it with LNP@mRNA or LNP@mRNA plus Fluzone Quadrivalent influenza vaccine (FluZ) group. As shown in fig. S9 (G to I), mice vaccinated with Flu-RBD showed significantly greater viral clearance than those vaccinated with LNP@mRNA or LNP@mRNA plus FluZ, suggesting that Flu-RBD provided more efficient protection against viral infection.

Having demonstrated that Flu-RBD has the capacity to induce RBD-specific antibody response, we next studied whether Flu-RBD preserved the immunogenicity as a flu vaccine. As shown in Fig. 3G, Flu-RBD induced comparable HA antibody titer to that of Flu or Flu-M-RBD group, as well as resulted in a similar T_H1-skewing immune response by a predominant induction of IgG2a antibody rather than IgG1 antibody (Fig. 3H). Restimulation by a HA peptide pool induced a higher population of IFN-γ^+ CD4 T cells and IFN-γ^+ CD8 T cells than IL-4^+ or IL-$17a^+$ CD4 and CD8 T cells for Flu-RBD vaccinations (Fig. 3, I and J), indicative of a robust production of T_H1-biased immune response. In addition, a higher level of IL-$17a^+$ CD4 and CD8 T cells was observed in Flu-RBD group relative to free Flu group. These results demonstrated that the modification of RBD antigen did not compromise the efficacy of Flu vaccine element. Furthermore, we found that Flu-RBD produced some amount of both RBD-specific and HA-specific IgA Abs in bronchoalveolar lavage fluid (BALF) of mice (fig. S10), indicating that Flu-RBD has potential to provide protection at or near the site of SARS-CoV-2 infection.

DC activation in the spleen and LNs by Flu-RBD vaccinations

Dendritic cells (DCs) are potent APCs and their activation prompts the priming of immunity mediators for B cells and T cells (*35*). To assess DC activation in response to our Flu-RBD vaccine, murine splenocytes and lymphocytes were isolated from mice that received two vaccinations. A higher percentage of $CD86^+$, $CD40^+$, and $CD80^+$ cells presented in both splenocytes and lymphocytes vaccinated with Flu-RBD group (figs. S11 and S12). Free RBD vaccinations significantly up-regulated the expression of $CD40^+$ compared to Flu vaccinations, whereas the frequency of cells expressing $CD80^+$ was drastically increased in Flu-vaccinated mice. Flu-RBD vaccinations induced the highest percentage of $CD40^+$ cells and a comparable percentage of $CD80^+$ cells with Flu vaccinations in both splenocytes and lymphocytes, suggesting a high degree of DC activation.

Cellular immune response and systemic cytokine stimulation by Flu-RBD vaccinations

Cellular immune responses were evaluated in splenocytes from vaccinated mice via induction of IFN-γ secretion after exposure to RBD and HA peptide pools (Fig. 4A). Flu-RBD vaccinations induced significantly higher levels of IFN-γ secretion relative to RBD, Flu, or Flu-M-RBD group, eliciting approximately 300 spot-forming units (SFU) per million splenocytes (Fig. 4, B and C). Like results in IFN-γ enzyme-linked immunosorbent spot (ELISpot) assay, Flu-RBD vaccinations stimulated the highest levels of IL-6 and tumor necrosis factor–α (TNF-α) secretion, whereas in RBD, Flu, and Flu-M-RBD groups, relatively lower levels of IL-6 and TNF-α were discovered (Fig. 4, D and E). The higher level of IL-6 may contribute to the induction of a T_H17 immune response for Flu-RBD group (*36*). These results indicated that Flu-RBD vaccines induced a robust cellular immune response, which could protect the hosts from viral replication.

Live SARS-CoV-2 challenge in hamsters with Flu-RBD vaccinations

The Syrian golden hamster model resembles severe clinical diseases of COVID-19 observed in humans, with rapid weight loss and severe lung pathology (*37*–*39*), which was used to assess the protection potency of Flu-RBD vaccine. After two doses of vaccinations, Syrian golden hamsters were challenged with live SARS-CoV-2 via intranasal route (Fig. 5A). Viral RNA levels in bronchoalveolar lavage (BAL) and oral swabs (OS) were evaluated by quantitative reverse transcription polymerase chain reaction (qRT-PCR; Fig. 5, B and C). At 2 days postinoculation (dpi), all immunized groups of PBS, Flu, Flu-M-RBD, and Flu-RBD showed high levels of RNA copies with median peaks of 6.772, 6.512, 6.318, and 6.122 $\log_{10}$ RNA copies/ml, respectively (Fig. 5C). Notably, peak RNA level in Flu-RBD–immunized animals was markedly decreased with a median of 3.702 $\log_{10}$ RNA copies/ml in OS on 7 dpi, indicative of the efficient protection medicated by Flu-RBD. In accordance with OS results, fewer copies of viral RNA with 2.568 $\log_{10}$ RNA copies/ml were tested in the BAL of Flu-RBD–vaccinated hamsters, much lower than that of PBS (5.916)–, Flu (5.906)–, and Flu-M-RBD (5.526)–vaccinated hamsters (Fig. 5B). Furthermore, RBD-specific IgG antibody titer was increased after SARS-CoV-2 infection in hamsters vaccinated with Flu-RBD (Fig. 5D). However, no significant increase in IgG antibody titer was observed for the hamsters who vaccinated with Flu-M-RBD (fig. S13). We further found that Flu-RBD vaccinations elicited 1.35 $\log_{10}$ fold higher median enzyme-linked immunosorbent assay (ELISA) titers in response to RBD than Flu-M-RBD at 7 dpi (Fig. 5E). Moreover, Flu-RBD induced comparable HA-specific antibody titers with free Flu or Flu-M-RBD (Fig. 5F). Clinical chemistry and hematological parameters of hamsters vaccinated with Flu-RBD remained within normal ranges (fig. S14).

Histopathological examinations revealed that the hamsters received PBS or Flu vaccinations had severe pulmonary lesions with multifocal necrotizing bronchiolitis, remarkable inflammatory infiltrates in the alveolar walls and air spaces, as well as pulmonary edema as compared to sham hamsters′ lung (Fig. 5, G and H). This pattern with dim amelioration was seen in the hamsters vaccinated with Flu-M-RBD. Comparatively, the hamsters vaccinated with Flu-RBD had obviously alleviated pneumonia symptoms. The resolution of pulmonary alveolus was improved with extended across larger areas, and a significant reduction in the number of polymorphonuclear and neutrophils was observed. Masson trichrome staining and Ashcroft score results revealed that Flu-RBD immunizations could diminish lung fibrosis with the preservation

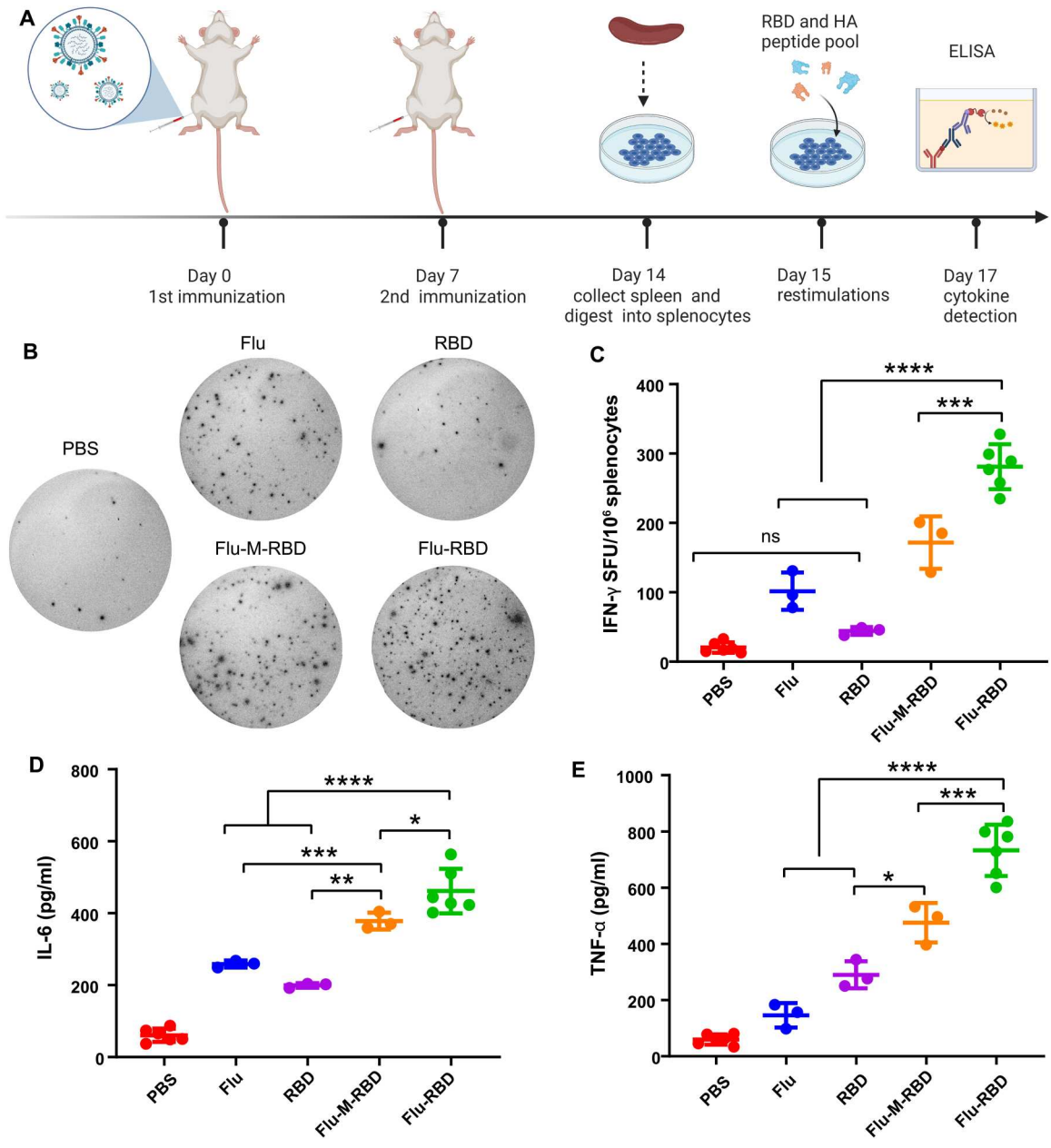

Fig. 4. Systemic cytokines secretion in Flu-RBD–vaccinated mice. (**A**) Schematic diagram of the animal experiment design for cellular immunity analysis. (**B**) Representative images of IFN-γ spots in vaccinated splenocytes after restimulation of RBD and HA peptide pools. (**C**) IFN-γ SFU numbers per 10^6 splenocytes as measured by ELISpot. Cytokines IL-6 (**D**) and TNF-α (**E**) secretion from splenocytes were assessed by ELISA. Data are mean ± SD. $n = 3$ or 6. Statistical analysis was performed by one-way ANOVA test with Bonferroni correction. *$P < 0.05$; **$P < 0.01$; ***$P < 0.001$; ****$P < 0.0001$. All replicates are biological.

of alveolar epithelial structures as compared to Flu or Flu-M-RBD vaccination (Fig. 5, I and J).

Histopathological examinations of Flu-RBD–vaccinated lungs

We further assessed the local distribution of SARS-CoV-2 within lung and found that SARS nucleocapsid (SARS-N) protein was prevalent in epithelial cells lining the bronchioles and alveoli (Fig. 6A). Frequently, the SARS-N–positive cells were found to co-localize with pan-cytokeratin marker, indicating that they mainly infected alveolar epithelial cells (Fig. 6B) (*40*). In addition, the cells infected with foci of the virus were accompanied by large inflammatory infiltrates of activated ionized calcium binding adaptor (Iba-1^+) or $CD206^+$ cells (Fig. 6C). In situ RNA hybridization (RNAscope) analysis showed that the lowest levels of both positive-sense and negative-sense viral RNA were presented in Flu-RBD immunization group rather than Flu or Flu-M-RBD group (Fig. 6D). In addition, we found that vaccinated hamsters with Flu-RBD significantly reduced inflammation infiltrates as reflected by less myeloperoxidase (MPO)–positive neutrophils in lung as compared to Flu or Flu-M-RBD vaccinations (Fig. 6E). Diffuse

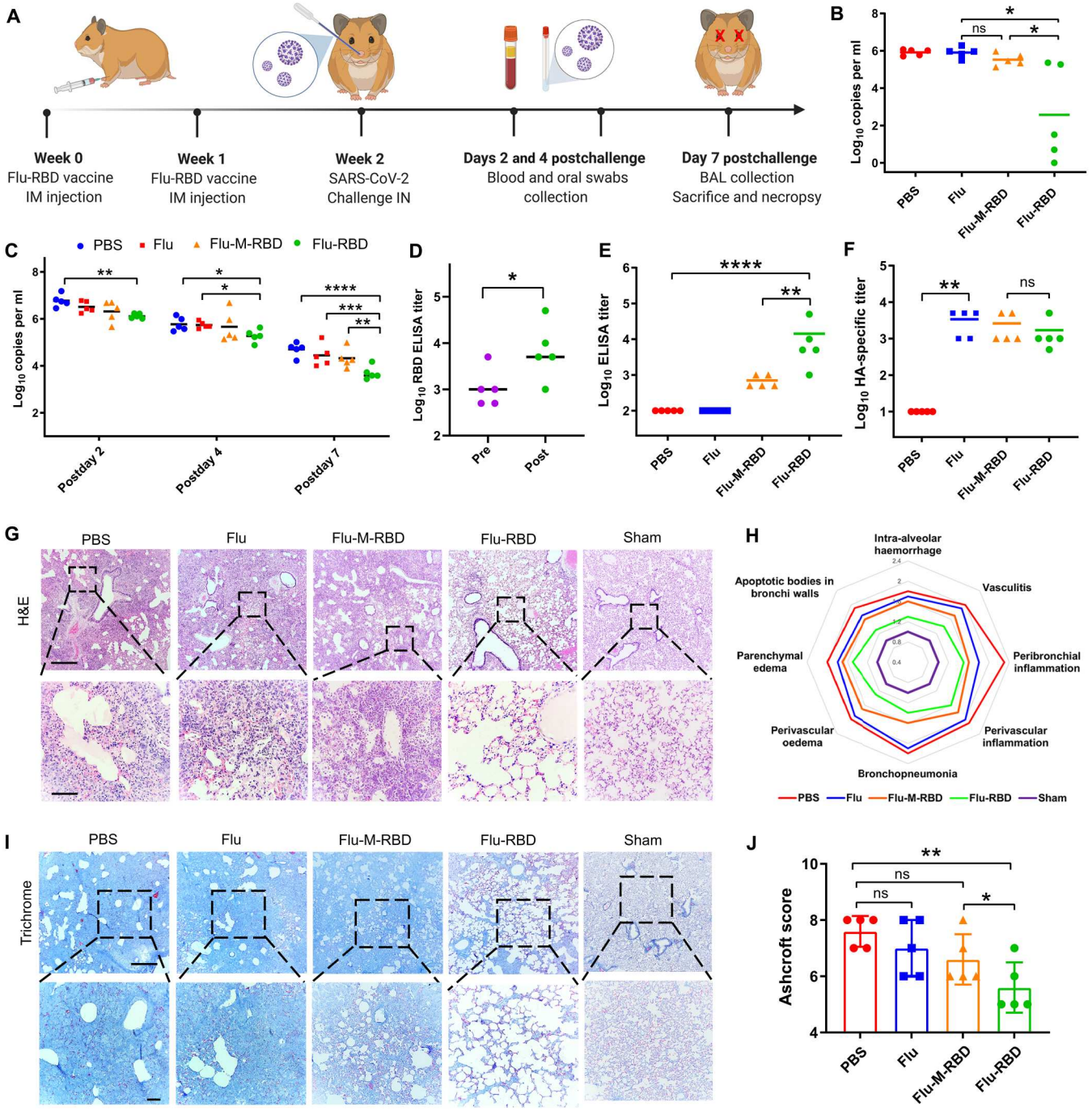

Fig. 5. Protective effects of Flu-RBD VLP vaccine in the Syrian hamster model against live SARS-CoV-2 infection. (**A**) Schematic illustrating the animal study design. IM, intramusular; IN, intranasal administration. (**B**) Viral RNA in BAL fluid from vaccinated hamsters at 7 dpi. (**C**) Viral RNA in OS from vaccinated hamsters at the indicated time points. (**D**) Quantification of RBD-specific IgG antibody titer from prechallenge and postchallenge hamsters with Flu-RBD immunizations. Quantification of RBD-specific (**E**) and HA-specific (**F**) binding IgG antibody titers from hamster serum detected by ELISA at 7 dpi. (**G**) Hematoxylin and eosin (H&E) images of representative lung sections at 7 dpi. Scale bars, 500 μm (top) and 100 μm (bottom). (**H**) Spider web plot displaying histopathological scoring of lung damage, normalized to sham hamsters (purple). (**I**) Masson's trichrome staining of lung sections at 7 dpi. Scale bars, 500 μm (top) and 100 μm (bottom). (**J**) Evaluation of lung fibrosis of hamsters using Ashcroft scoring assay, which was performed blindly. Each dot represents data from one animal. Data are mean ± SD. $n = 5$. Statistical analysis was performed by one-way ANOVA test with Bonferroni correction. *$P < 0.05$; **$P < 0.01$; ***$P < 0.001$; ****$P < 0.0001$. All replicates are biological.

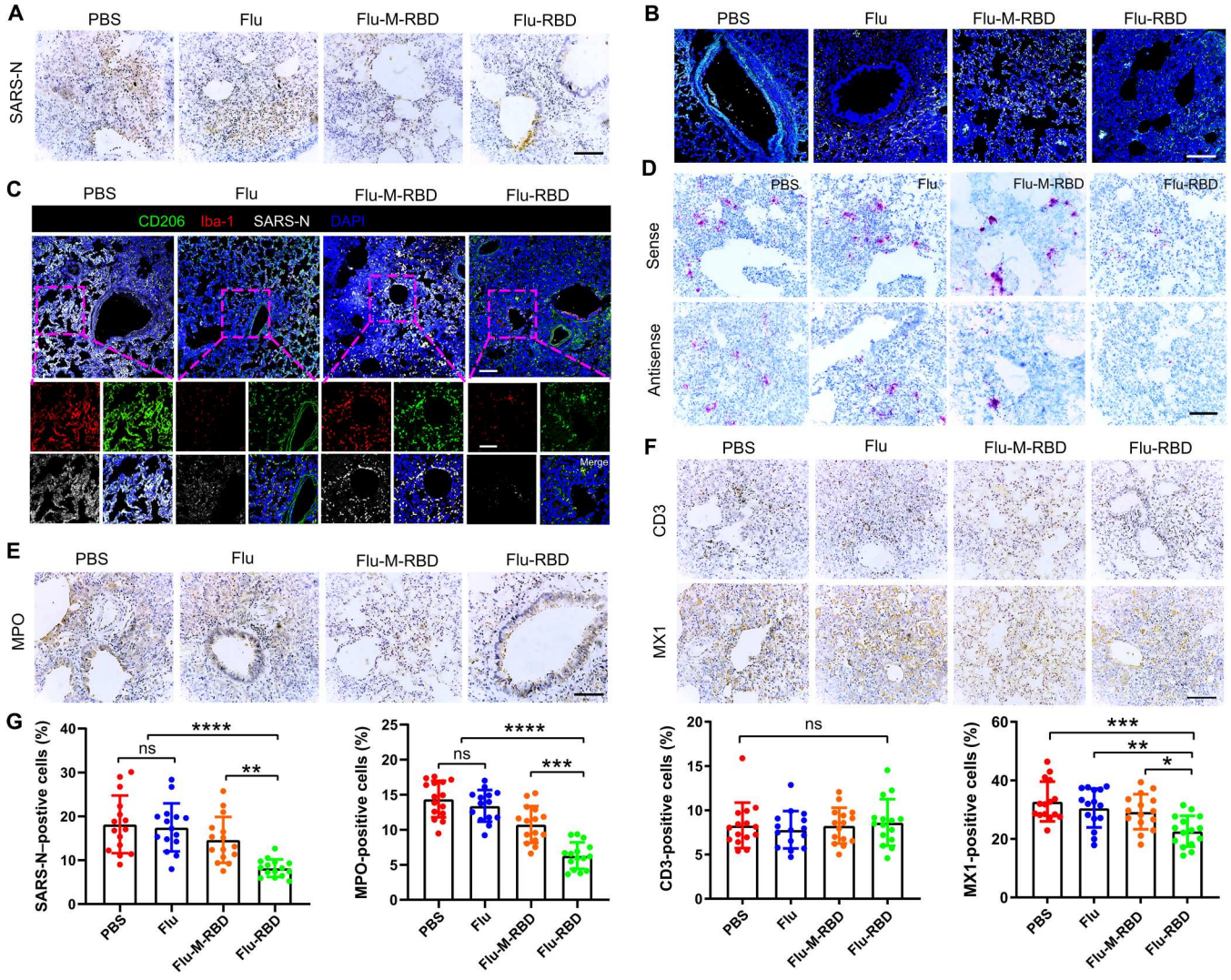

Fig. 6. Histopathological changes and RNAscope analysis of Syrian hamsters vaccinated with Flu-RBD. (**A**) Immunohistochemistry (IHC) images of SARS-N expression in lung tissues of vaccinated hamsters 7 dpi. Scale bar, 100 μm. (**B**) Evaluation of local distribution of SARS-N in lung tissues of hamsters. SARS-N (red), pan-cytokeratin (greeen). Scale bar, 50 μm. (**C**) Immunofluorescence staining of SARS-N, Iba-1 and CD206 of lung tissues in hamsters 7 dpi. Scale bars, 50 μm. (**D**) RNAscope images revealing regional distribution and levels of viral RNA in lung tissues. Scale bar, 100 μm. Representative images of MPO (**E**), as well as CD3 T lymphocytes (**F**) and MX1 (F) IHC staining of hamster lungs 7 dpi. Scale bars, 100 μm. (**G**) Quantification of positive SARS-N, MPO, CD3 and MX1 cell percentages in lung sections of hamsters. Each dot represents data from one image file, $n = 15$. Data are mean ± SD. Statistical analysis was performed by one-way ANOVA test with Bonferroni correction. $^{*}P < 0.05$; $^{**}P < 0.01$; $^{***}P < 0.001$; $^{****}P < 0.0001$. Analysis in (G) represents technical replicates from five independent biological samples.

expression of $CD3^{+}$ T lymphocytes was evaluated in lungs (Fig. 6F), showing no notable changes among PBS, Flu, Flu-M-RBD, and Flu-RBD groups (Fig. 6G). We further discovered the obvious down-regulation of MX1, an IFN-induced antiviral protein against a wide range of RNA viruses (*41*), in the hamsters vaccinated with Flu-RBD (Fig. 6, F and G), confirming the reduction of virus replication due to highly potent neutralizing antibody, in keeping with the lowest level of SARS-N expression in the animals immunized with Flu-RBD (Fig. 6G). Collectively, these results indicated that Flu-RBD immunizations effectively protected hamster against SARS-CoV-2 infection.

Protective activity of Flu-RBD against SARS-CoV-2 Delta pseudovirus

SARS-CoV-2 Delta (B.1.617.2) variant has been found to be more highly fusogenic and pathogenic than ancestral SARS-CoV-2 (*42*–*44*), which was used to evaluate the cross-protection activity of Flu-RBD vaccine against SARS-CoV-2 variants. Seven days after two immunizations, the mice were challenged with RFP and luciferase-expressing SARS-CoV-2 Delta pseudovirus via intranasal route (Fig. 7A). Ex vivo imaging results in Fig. 7B revealed that the bright RFP signal was observed in the mice vaccinated with RBD or Flu-M-RBD group. In contrast, Flu-RBD vaccinations remarkably decreased the RFP signal in lung (Fig. 7, B and C), showing a stronger cross-variant neutralization ability. Confocal imaging of the whole lungs revealed that, in the Flu-RBD group, a

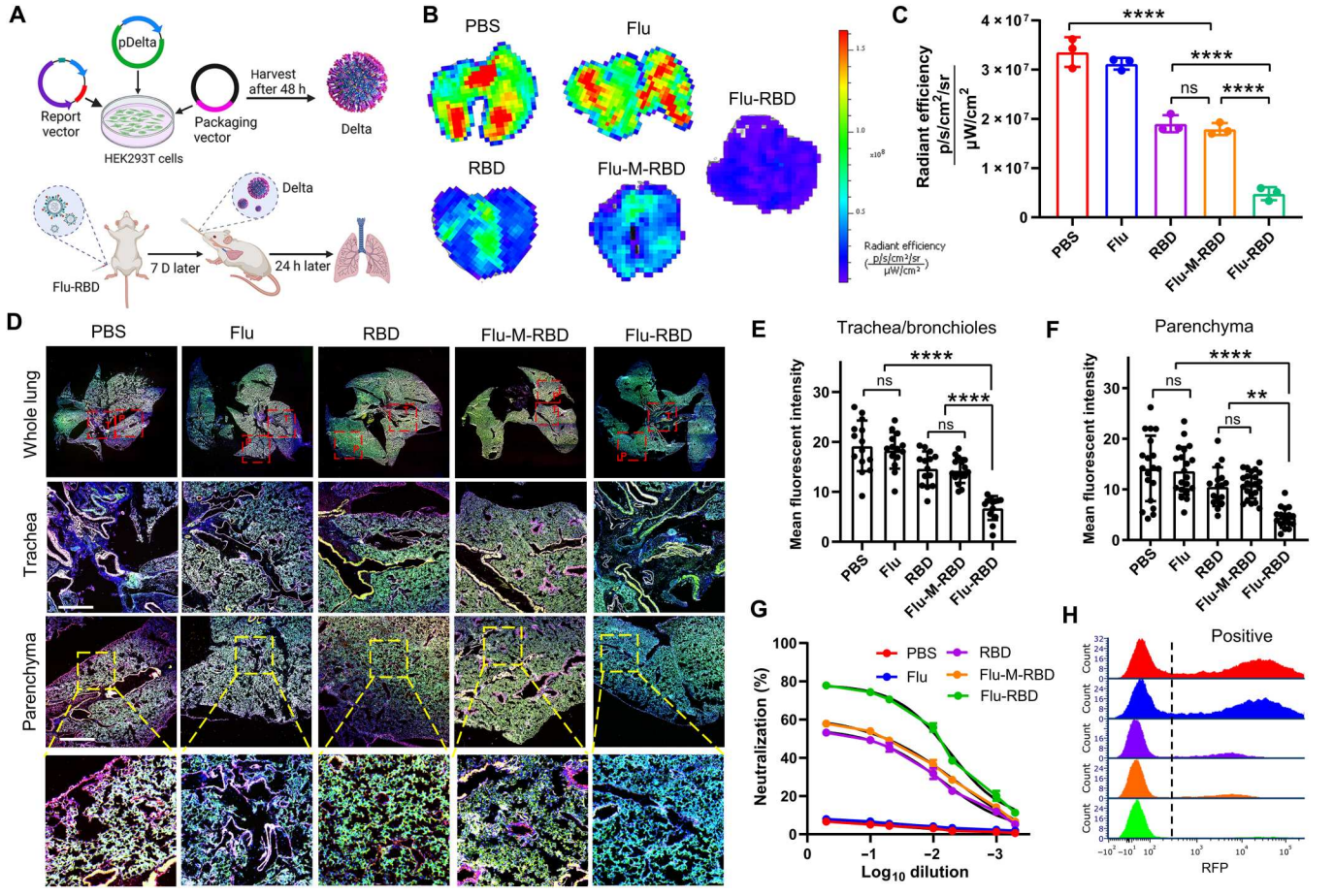

Fig. 7. Flu-RBD vaccinations inhibit the infections of SARS-CoV-2 Delta pseudovirus in mice. (**A**) Schematic illustrating Delta pseudovirus construction and the animal study design. D, days; h, hours. (**B**) Representative lung tissue images from immunized mice inoculated with SARS-CoV-2 Delta pseudovirus with an RFP reporter. (**C**) Quantification of the integrated RFP density in ex-vivo mouse lungs. $n = 3$. (**D**) Immunostaining imaging of whole lung of vaccinated mice for DAPI (blue), phalloidin (green), and SARS-CoV-2 Delta pseudovirus (red). Scale bar, 400 μm. Quantification of mean fluorescence intensity of RFP in tracheal/bronchial (**E**) and parenchymal (**F**) tiles from whole lung images. Each dot represents data from one image tile, $n = 13$ to 25. (**G**) Neutralization curves of mouse sera against SARS-CoV-2 Delta pseudovirus in A549 cells expressing ACE2. $n = 3$. (**H**) Flow plots of SARS-CoV-2 Delta pseudovirus incubated with A549 cells, which was inhibited by sera from vaccinated mice. Data are mean ± SD. Statistical analysis was performed by one-way ANOVA test with Bonferroni correction. $^{**}P < 0.01$; $^{****}P < 0.0001$. The replicates in (C) and (G) are biological. Analysis in (E) and (F) represents technical replicates from three independent biological samples.

lower amount of SARS-CoV-2 Delta pseudovirus was distributed in both the trachea/bronchioles and parenchyma compared to the free RBD or Flu-M-RBD vaccination groups (Fig. 7, D to F). We further evaluated the neutralization properties of sera from vaccinated mice using A549 cells expressing ACE2. As illustrated in Fig. 7G, the sera collected from Flu-RBD group efficiently blocked the infection of A549 cells expressing ACE2 by SARS-CoV-2 Delta pseudovirus. The half-maximal inhibitory dilution of sera from Flu-RBD vaccinations was determined to be 0.0085, significantly lower than that of RBD vaccinations (0.127) and Flu-M-RBD vaccinations (0.0665). Flow cytometry analysis further demonstrated that the sera (0.5 dilution) stemmed from mice with Flu-RBD vaccinations could efficiently prevent SARS-CoV-2 Delta pseudovirus entry into A549 cells (Fig. 7H). Collectively, these compound datasets demonstrated that Flu-RBD shows a high potent neutralization effect against the continued emergence of SARS-CoV-2 variants.

Protective activity of Flu-RBD against wild-type influenza A H1N1 inactivated virus

Last, we studied the protection efficacy of Flu-RBD vaccine against wild-type influenza A H1N1 inactivated virus with red fluorescence. Compared to PBS control, Flu-RBD vaccinations efficiently accelerated the clearance of H1N1 inactivated virus in mice (fig. S15), suggesting the preservation of the immunogenicity of Flu vaccine. Furthermore, we compared the neutralization activity of Flu-RBD with clinical standard vaccine LNP@mRNA plus FluZ and found that Flu-RBD vaccine's protection efficacy against H1N1 inactivated virus was similar to that of the LNP@mRNA plus FluZ group, indicating the potential of Flu-RBD vaccine for preventing flu infection (fig. S15). We next assessed whether there is improved protection activity when using the booster immunization regimen. As illustrated in fig. S16, mice immunized with the booster regimen had substantially higher level of RBD-specific IgG and HA-specific IgG antibody titers in serum compared to the prime regimen. These findings suggest that a booster dose of Flu-RBD significantly

augmented immune responses and protective activity against COVID-19 or influenza infection.

DISCUSSION

To date, none of the 14 recommended treatments such as remdesivir, hydroxychloroquine, and IFN showed significant impact on overall mortality or hospital length of stay in COVID-19 hospitalized patients (*45*). Therefore, safe, effective, and widely available vaccines are essential to eliminating COVID-19 pandemic (*46*). Despite that multiple SARS-CoV-2 vaccine candidates have been approved for emergency usage by using conventional viral, immunogens, and genetic (DNA and mRNA) approaches (*30*, *47*, *48*), none of them is constructed to protect the public against COVID-19/flu coinfection, which is difficult to distinguish regarding their similar clinical presentations (*6*, *49*). Of special note, influenza A virus pre-infection strongly enhances the infectivity of SARS-CoV-2 by increasing virus entry, resulting in a higher mortality rate. Some clinical reports indicated that the trained immunity induced by influenza vaccines could lead to some degree of protection against COVID-19. Those who got an influenza vaccine that were 30% less likely to be infected by SARS-CoV-2, and 89% less likely to evolve serious COVID-19 relative to those who did not receive the influenza vaccine (*50*). Here, we developed a promising vaccine candidate with two-hit protection against both SARS-CoV-2 and flu infections. RBD is the primary target of neutralization potency in COVID-19 human convalescent sera (*13*). RBD-based subunit vaccines have shown to be efficient and promising in preclinical studies by producing a SARS-CoV-2–specific antibody response (*51*). Inactivated influenza A H1N1 virus (Flu) vaccine against influenza has been developed for decades and demonstrated to be effective and safe even for pregnant women (*52*). Inspired by their advantages, we conjugated the RBD of SARS-CoV-2 with Flu as a two-hit vaccine.

We found that Flu-RBD led to a significantly greater shift in RBD distribution from injection site toward LNs by 24 hours than free RBD in mice. Moreover, Flu-RBD prolonged the retention of RBD in the draining LNs and enhanced the internalization of RBD by APCs, revealing that Flu could function as an efficient platform for delivery of RBD into LNs. Accordingly, Flu-RBD vaccinations produced a higher titer of RBD-specific IgG Abs compared to RBD. Furthermore, Flu-RBD vaccine preserved the immunogenicity of Flu vaccine by generating HA-specific IgG Abs and T cell responses, which play key roles against viral invasion. Collectively, our results showed that Flu-RBD VLP vaccine could evoke both RBD and HA specific immune responses.

We used Syrian golden hamsters, an animal model for studying SARS-CoV-2 pathogenesis and transmission (*37*), to investigate the safety and efficacy of Flu-RBD vaccine. Vaccinations of hamsters with two doses of Flu-RBD provided effective protective immunities against SARS-CoV-2 infection as demonstrated by reduced viral load and high level of antibody titers. Histopathological analysis of lung tissues from hamsters vaccinated with Flu-RBD exhibited minimal lung pathology and low numbers of SARS-CoV-2 infected cells as opposed to SARS-CoV-2 infected hamsters, showing intensive damage and stronger SARS-CoV-2 signals.

Continued emergence of SARS-CoV-2 variants poses severe threats to present COVID-19 vaccines, particularly as the Delta variant (B.617.2) that causes sharp rises in infections in many countries, even some with relatively high vaccination coverage (*43*). Our results suggested that vaccinations with two doses of Flu-RBD could elicit potent neutralization activity against SARS-CoV-2 Delta pseudovirus. Furthermore, the serum from mice vaccinated with Flu-RBD efficiently blocked the Delta pseudovirus entry into host cells, indicative of its strong cross-protective capacity.

With more scientists predicting that SARS-CoV-2 is expected to become endemic and adopt a seasonal pattern of annual epidemics, several recent clinical trials combing SARS-CoV-2 vaccine with the annual influenza vaccine have been conducted to evaluate their safety and potential against COVID-19/influenza infection (*53*–*55*). In a phase 3 trial conducted by Novavax, coadministration of NVX-CoV2373 with influenza vaccine has proven safe, with a reactogenicity profile similar to that of either vaccine administered alone (*53*). In a phase 4 trial, concomitant administration of ChAdOx1 (Oxford-AstraZeneca) or BNT162b2 (BioNTech) with influenza vaccine did not raise any safety concerns and preserved antibody responses to both vaccines (*54*). In another phase 2 trial, interim results showed that no safety concerns for concomitant administration of mRNA-1273 vaccine with influenza vaccine in elderly individuals (*55*). Although promising, these strategies were simply combo. We presented an alternative strategy with the development of a single vaccine efficiently targeting two respiratory viruses, SARS-CoV-2 and influenza, which is more cost-effective, enhanced immunogenicity, improved patient convenience, and fewer missed opportunities to vaccinate over the reported strategies.

A limitation of our study is that we did not study the protective activity of Flu-RBD against live Flu infection in an animal model, and future studies are planned to evaluate this question. However, it is worth noting that Flu-RBD vaccine maintained the immunogenicity of flu vaccine by generating HA-specific IgG antibody in both mice and hamsters and HA-specific T cell responses, as well as showing great capacity against wild-type influenza A H1N1 inactivated virus infection. In summary, we developed a two-hit protection vaccine against SARS-CoV-2/flu infections based on RBD conjugated with inactivated influenza A virus. This two-in-one vaccine improves immunogenicity of RBD antigen, reduces vaccine hesitancy, as well as eases the public's fatigue toward vaccinations and reduces the burden on health care services for vaccine delivery. We expect that our two-hit VLP vaccine will provide important insights into developing safe and effective vaccines for targeting coinfection of circulating viral threats.

MATERIALS AND METHODS

Synthesis of Flu-RBD

Before preparing Flu-RBD, RBD were reacted with AZO-PEG-NHS (PG2-AZNS-3k, NANOCS). Briefly, 10 μg of recombinant SARS-CoV-2 RBD protein (40592-V08B, Sino Biological) was reconstituted and dropped into AZO-PEG-NHS solution (2 mg/ml) and reacted for 24 hours at 4°C to form RBD-PEG-AZO. To remove unreacted AZO-PEG-NHS, the above mixture was dialyzed using Slide-A-Lyzer MINI Dialysis Units [10,000 molecular weight cutoff (MWCO)] and concentrated by Amicon Ultra-4 filter (10-kDa cutoff).

Meanwhile, inactivated influenza A (H1N1) virus (23-047-299, Thermo Fisher Scientific) defined as Flu was reacted with DBCO-PEG-NHS (PG2-DBNS-5k, NANOCS) at 4°C for 24 hours to

generate DBCO-PEG-Flu. Unreacted DBCO-PEG-NHS removal was performed by centrifugation via Amicon Ultra-4 filter (100 kDa). To synthesize Flu-RBD, 10 μg of RBD-PEG-AZO was added into 10^{11} of DBCO-PEG-Flu solution and reacted at 4°C for overnight. The resultant Flu-RBD was ultracentrifugated at 100,000*g* for 70 min at 4°C and washed with PBS twice (10 mM, pH 7.4) and resuspension in PBS buffer. To quantify the number of RBD protein on Flu-RBD, 10^5 of Flu-RBD particles were lysed by radioimmunoprecipitation assay buffer and quantification via an ELISA assay (EH492RB, Thermo Fisher Scientific).

Synthesis of RBD-RhB and Flu-RBD-RhB

One hundred micrograms of NHS-RhB (186-1425, Thermo Fisher Scientific) was reacted with 10 μg of RBD in PBS buffer at 4°C overnight. Free NHS-RhB removal was performed by centrifugation and washed with PBS buffer three times via Amicon Ultra-0.5 filter (10-kDa cutoff). RBD-RhB was mixed with AZO-PEG-NHS to generate RBD-PEG-AZO-RhB and then reacted with DBCO-PEG-Flu to synthesize Flu-RBD-RhB according to above methods.

Preparation of mRNA of full-length spike protein and its loading in lipids

The S protein plasmid for in vitro transcription was created using the full-length DNA sequence of the trimerized S surface glycoprotein (Gene Bank: QHD43416.1; amino acids 1 to 1273) of the SARS-CoV-2 isolate Wuhan-Hu-1. The mRNA construct of S protein was prepared, extracted, and purified according to our previous report (*56*). Purified mRNA was formulated with lipids (ALC-3015, ALC-0159, 1,2-distearoyl-sn-glycero-3-phosphocholine (DSPC), and cholesterol) using the ethanol-drop process to obtain RNA-lipid nanoparticles (LNP@mRNA) according to Pfizer's report (*32*). The molar ratios of the ALC-3015:ALC-0159:cholesterol:DSPC used are 46.3:1.6:42.7:9.4, and each dose of LNP@mRNA vaccine consists of 0.43 mg of ALC-3015, 0.05 mg of ALC-0159, 0.09 mg of DSPC, 0.19 mg of cholesterol, and 30 μg of mRNA according to the released document from Pfizer (*34*).

Animal procedures

With respect to World Organization for Animal Health recommendation, CD1 mice are strain for the vaccine potency assay in mouse (*57*), which have been used for evaluating the immunogenicity of various vaccines including RB51 vaccine, Zika vaccine, PCV15 vaccine, etc. Accordingly, female CD1 mice [Crl:CD1(ICR)] that are 6 to 8 weeks old and purchased from Charles River Laboratory (MA, USA) were used for assessing the immunogenicity of Flu-RBD vaccine. All animal studies were compliant with the Institutional Animal Care and Use Committee (IACUC) at North Carolina State University (protocol # 19-806-B). RBD-RhB and Flu-RBD-RhB were administered into the right hint limb of mice via i.m. injection. After 4 or 24 hours postinjection, the right, left, and cervical draining LNs as well as major organs were harvested and imaged via the Xenogen Live Imager (PerkinElmer, MA, USA).

PBS, Flu (10^{10}/kg), RBD (0.71 μg/kg), Flu-RBD (10^{10}/kg), and the mixture of Flu and RBD (Flu-M-RBD) vaccinations were i.m. injected with two doses 1 week apart. Seven days later, blood, spleen, BALF, and LNs were collected for further analysis. To evaluate the immune responses of booster, CD1 mice administrated with two doses of Flu-RBD (prime) were received a homologous booster dose 4 weeks later. Seven days later, the blood of mice was collected for further analysis.

IgG antibody titer

One hundred microliters of RBD or influenza A H1N1 HA recombinant protein (4 μg/ml; A42579, Thermo Fisher Scientific) was added into micro titer plates (Nunc Cell Culture, Thermo Fisher Scientific) for overnight at 4°C. After that, 200 μl of 5% (w/v) bovine serum albumin (B6717, Sigma-Aldrich) in phosphate-buffered saline with 0.1% Tween 20 (PBS-T) buffer was added to each well to block nonspecific binding and incubated at 37°C for 1 hour. After three times of wash with PBS-T, serum samples with serial dilutions (1:100, 1:1000, 1:3000, 1:5000, 1:10,000, 1:50,000, 1:100,000, and 1:200,000) and control serum samples (1:100 dilution) were added to the wells and incubated at 37°C for 1.5 hours. After washing intensively, 100 μl of horseradish peroxidase–labeled anti-mouse IgG secondary antibody with 1:10,000 dilution was added for 1 hour of incubation at 37°C. After three times of wash, 100 μl of trimethylboron was added into each well and incubated at room temperature for 30 min. Fifty microliters of 2 M H_2SO_4 (Sigma-Aldrich) was used for stopping the reaction, and the optical absorption was determined at 450 nm via a plate reader. The endpoint IgG titer was determined as the highest reciprocal dilution of serum that exhibits an optical density greater than twofold of the mean control group.

Cytokine measurements in splenocytes

Splenocytes from each vaccinated mouse were seeded in an ELISpot plate (EL485, R&D Systems) (10^6 cells per well) and stimulated with RBD peptide pool (PP002-A, SinoBiological) and H1N1 HA peptide pool (130-097-285, Miltenyi Biotec). Antigen-specific cells secreting IFN-γ were detected according to the protocol of the manufacturer. The formed SFUs were imaged by an anatomical microscope (Nikon, Minato City, Tokyo, Japan) and counted by ImageJ software. Furthermore, the collected splenocytes were also plated in six-well plates (5×10^6 per well) and restimulated with RBD peptide pool and H1N1 HA peptide pool. After 48 hours of incubation, the culture supernatant was collected. The Mouse IL-6 Kit (RAB0308, Sigma-Aldrich) and the Tumor Necrosis Factor α Kit (RAB0477, Sigma-Aldrich) were used to detect IL-6 and TNF-α levels from collected supernatant.

T cell immunities in splenocytes

At day 7 postprime, mouse splenocytes were collected and seeded to the plate (1×10^6 per well). The RBD peptide pool or influenza A HA peptide pool was added to stimulate splenocytes for 12 hours at 37°C, respectively. Brefeldin A solution was added into the plate with a final concentration of 1 μg/ml and incubated for another 4 hours. Following that, the splenocytes were collected and stained with CD4–fluorescein isothiocyanate (FITC) (100406, BioLegend) antibody or CD8-FITC (ab22504, Abcam) antibody at a dilution of 1:100. After washing with magnetic-activated cell sorting flow buffer, splenocytes were fixed with 4% paraformaldehyde (PFA) and permeabilized using saponin and incubated with IFN-γ–phycoerythrin (PE) (507806, BioLegend), IL-4–PE (504103, BioLegend), or IL-17a–APC (17-7177-81, Invitrogen) Abs for 1 hour. The stained splenocytes were analyzed by a CytoFLEX flow cytometer (Beckman Coulter). Data analyses were carried out by FCS Express V6.

Syrian golden hamster studies with live SARS-CoV-2

Six to 8 weeks old of 20 male and female Syrian golden hamsters (Envigo) were randomly assigned to four groups and housed at

Bioqual. Hamsters were i.m. administered with two doses of PBS, Flu (10^{10}/kg) or Flu-M-RBD, Flu-RBD (10^{10}/kg) at week 0 and week 1 ($n = 5$ per group, 2 females/3 males). At week 2, the hamsters were challenged with 100 μl of 2×10^4 50% tissue culture infective dose SARS-CoV-2 via intranasal routes (50 μl in each nare). BAL, OS, and blood were harvested at the indicated time. All hamster experiments were conducted in accordance with all relevant local, state, and federal regulations that were approved by the Bioqual IACUC (20-091P).

Viral load assay

Following procedures previously described by Duke Human Vaccine Institute (*58*), SARS-CoV-2 RNA copies per milliliter were tested by qRT-PCR assay. Briefly, viral RNA was extracted using the QIAsymphony SP sample preparation platform with the DSP Virus/Pathogen Midi Kits (Qiagen). A primer specific to SARS-CoV-2 envelope gene was annealed to extracted RNA, which was reverse-transcribed into cDNA using SuperScript III Reverse Transcriptase and RNaseOut. The cDNA was treated with ribonuclease and then added to the custom 4× TaqMan Gene Expression Master Mix including primers and a fluorescently labeled hydrolysis probe. The qRT-PCR reaction was performed on a QuantStudio 3 Real-Time PCR system. SARS-CoV-2 RNA copies per reaction were interpolated via quantification cycle data and a serial dilution of a highly characterized custom DNA plasmid with SARS-CoV-2 envelope gene sequence. The limit of quantification for the assay was approximately 62 RNA copies/ml of sample.

SARS-CoV-2 Delta pseudovirus neutralization assay

SARS-CoV-2 Delta pseudoviruses were constructed by cotransfecting HEK293T cells with the plasmids of plv-spike-v8 (InvivoGen), pLenti-EF1pluciferase-PGK-RFP-T2A-PURO lentiviral reporter (LR252, ALSTEM), and pspax2 (64586, addgene) via Lipo3000 (L3000015, Thermo Fisher Scientific). After 48 to 72 hours, Delta pseudoviruses were harvested from culture medium through centrifugation (3000 rpm, 10 min), aliquoted, and stored at −80°C before use.

Seven-week-old female CD1 mice were vaccinated with two doses of PBS, RBD, Flu, Flu-M-RBD, or Flu-RBD once a week. Seven days later, mice were inoculated with SARS-CoV-2 Delta pseudovirus carrying both RFP and luciferase reporters. Lung organs were harvested and imaged at 24 hours postchallenge by the Xenogen Live Imager. To study the distribution of Delta pseudovirus in the lung, the collected lung tissues were fixed in 4% PFA, dehydrated using 30% sucrose solution, and then frozen in O.C.T. compound (Tissue-Tek). Cryo-sections were permeabilized and blocked with Dako containing 0.1% saponin solution for 1 hour and then stained with phalloidin antibody (ab176753, Abcam). The ProLong Gold Antifade reagent with DAPI was used to counterstain nuclei and prevent the fade of the fluorophore. Imaging was performed via Olympus FLUOVIEW CLSM.

The sera samples from vaccinated mice were collected to assess their neutralization activity against SARS-CoV-2 Delta pseudovirus. A549 cells expressing human ACE2 and transmembrane serine protease 2 (TMPRSS2) were obtained from InvivoGen (a549-hace2tpsa). Sera samples with the indicated dilutions were incubated with SARS-CoV-2 Delta pseudovirus for 1 hour at 37°C. After that, the mixture was added in the A549 cells and incubated for another 24 hours. The luciferase signals from infected cells were determined by the Dual-Glo Luciferase Assay System (Promega). Furthermore, the A549 cells infected with the mixture of SARS-CoV-2 Delta with serum at a ratio of 1:1 were collected for flow cytometry analysis via the RFP reporter.

Wild-type influenza A H1N1 inactivated virus clearance assay

Wild-type influenza A H1N1 (VNV-019) inactivated virus was purchased from Creative Biogene and labeled with 1,1-Dioctadecyl-3,3,3,3-tetramethylindodicarbocyanine (DID) dye (V22887, Thermo Fisher Scientific). Seven-week-old female CD1 mice were i.m. administered with PBS, Flu-RBD, LNP@mRNA, or LNP@mRNA plus Fluz in two doses once a week. Seven days after two vaccinations, every mouse was challenged with H1N1 inactivated virus with red fluorescence. Lung organs were harvested and imaged at 24 hours postadministration by the Xenogen Live Imager. Immunofluorescence imaging of lung tissues was performed by an Olympus FLUOVIEW CLSM.

Statistical analysis

All experiments were performed at least three times independently. Results are shown as means ± SD. Comparisons between any two groups were performed using the two-tailed, unpaired Student's *t* test. Comparisons among multiple groups were performed using one-way analysis of variance (ANOVA), followed by the post hoc Bonferroni test. Group data were analyzed by two-way ANOVA with Tukey's multiple comparisons test. Single, double, triple, and four asterisks represent $P < 0.05$, 0.01, 0.001, and 0.0001, respectively; $P < 0.05$ was considered statistically significant.

Supplementary Materials

This PDF file includes:

Supplementary Text
Figs. S1 to S19

REFERENCES AND NOTES

1. C. Wang, P. W. Horby, F. G. Hayden, G. F. Gao, A novel coronavirus outbreak of global health concern. *Lancet* **395**, 470–473 (2020).
2. V. Kaushal, S. Srivastava, Hospitality and tourism industry amid COVID-19 pandemic: Perspectives on challenges and learnings from India. *Int. J. Hosp. Manag.* **92**, 102707 (2021).
3. R. van Aalst, S. Gravenstein, V. Mor, S. M. Mahmud, J. Wilschut, M. Postma, A. Chit, Comparative effectiveness of high dose versus adjuvanted influenza vaccine: A retrospective cohort study. *Vaccine* **38**, 372–379 (2020).
4. E. Cuadrado-Payán, E. Montagud-Marrahi, M. Torres-Elorza, M. Bodro, M. Blasco, E. Poch, A. Soriano, G. J. Piñeiro, SARS-CoV-2 and influenza virus co-infection. *Lancet* **395**, e84 (2020).
5. Y. Cheng, J. Ma, H. Wang, X. Wang, Z. Hu, H. Li, H. Zhang, X. Liu, Co-infection of influenza A virus and SARS-CoV-2: A retrospective cohort study. *J. Med. Virol.* **93**, 2947–2954 (2021).
6. S. Azekawa, H. Namkoong, K. Mitamura, Y. Kawaoka, F. Saito, Co-infection with SARS-CoV-2 and influenza A virus. *IDCases* **20**, e00775 (2020).
7. S. A. Hashemi, S. Safamanesh, H. Ghasemzadeh-Moghaddam, M. Ghafouri, A. Azimian, High prevalence of SARS-CoV-2 and influenza A virus (H1N1) coinfection in dead patients in Northeastern Iran. *J. Med. Virol.* **93**, 1008–1012 (2021).
8. L. Bai, Y. Zhao, J. Dong, S. Liang, M. Guo, X. Liu, X. Wang, Z. Huang, X. Sun, Z. Zhang, L. Dong, Q. Liu, Y. Zheng, D. Niu, M. Xiang, K. Song, J. Ye, W. Zheng, Z. Tang, M. Tang, Y. Zhou, C. Shen, M. Dai, L. Zhou, Y. Chen, H. Yan, K. Lan, K. Xu, Coinfection with influenza A virus enhances SARS-CoV-2 infectivity. *Cell Res.* **31**, 395–403 (2021).
9. J. Stowe, E. Tessier, H. Zhao, R. Guy, B. Muller-Pebody, M. Zambon, N. Andrews, M. Ramsay, J. Lopez Bernal, Interactions between SARS-CoV-2 and influenza, and the impact of co-infection on disease severity: A test-negative design. *Int. J. Epidemiol.* **50**, 1124–1133 (2021).
10. L. Dai, T. Zheng, K. Xu, Y. Han, L. Xu, E. Huang, Y. An, Y. Cheng, S. Li, M. Liu, M. Yang, Y. Li, H. Cheng, Y. Yuan, W. Zhang, C. Ke, G. Wong, J. Qi, C. Qin, J. Yan, G. F. Gao, A universal

design of betacoronavirus vaccines against COVID-19, MERS, and SARS. *Cell* **182**, 722–733.e11 (2020).

11. Q. Wang, Y. Zhang, L. Wu, S. Niu, C. Song, Z. Zhang, G. Lu, C. Qiao, Y. Hu, K. Y. Yuen, Q. Wang, H. Zhou, J. Yan, J. Qi, Structural and functional basis of SARS-CoV-2 entry by using human ACE2. *Cell* **181**, 894–904.e9 (2020).
12. P. J. M. Brouwer, T. G. Caniels, K. van der Straten, J. L. Snitselaar, Y. Aldon, S. Bangaru, J. L. Torres, N. M. A. Okba, M. Claireaux, G. Kerster, A. E. H. Bentlage, M. M. van Haaren, D. Guerra, J. A. Burger, E. E. Schermer, K. D. Verheul, N. van der Velde, A. van der Kooi, J. van Schooten, M. J. van Breemen, T. P. L. Bijl, K. Sliepen, A. Aartse, R. Derking, I. Bontjer, N. A. Kootstra, W. J. Wiersinga, G. Vidarsson, B. L. Haagmans, A. B. Ward, G. J. de Bree, R. W. Sanders, M. J. van Gils, Potent neutralizing antibodies from COVID-19 patients define multiple targets of vulnerability. *Science* **369**, 643–650 (2020).
13. A. C. Walls, B. Fiala, A. Schafer, S. Wrenn, M. N. Pham, M. Murphy, L. V. Tse, L. Shehata, M. A. O'Connor, C. Chen, M. J. Navarro, M. C. Miranda, D. Pettie, R. Ravichandran, J. C. Kraft, C. Ogohara, A. Palser, S. Chalk, E. C. Lee, K. Guerriero, E. Kepl, C. M. Chow, C. Sydeman, E. A. Hodge, B. Brown, J. T. Fuller, K. H. Dinnon 3rd, L. E. Gralinski, S. R. Leist, K. L. Gully, T. B. Lewis, M. Guttman, H. Y. Chu, K. K. Lee, D. H. Fuller, R. S. Baric, P. Kellam, L. Carter, M. Pepper, T. P. Sheahan, D. Veesler, N. P. King, Elicitation of potent neutralizing antibody responses by designed protein nanoparticle vaccines for SARS-CoV-2. *Cell* **183**, 1367–1382.e17 (2020).
14. C. Fougeroux, L. Goksøyr, M. Idorn, V. Soroka, S. K. Myeni, R. Dagil, C. M. Janitzek, M. Søgaard, K.-L. Aves, E. W. Horsted, S. M. Erdoğan, T. Gustavsson, J. Dorosz, S. Clemmensen, L. Fredsgaard, S. Thrane, E. E. Vidal-Calvo, P. Khalifé, T. M. Hulen, S. Choudhary, M. Theisen, S. K. Singh, A. Garcia-Senosiain, L. Van Oosten, G. Pijlman, B. Hierzberger, T. Domeyer, B. W. Nalewajek, A. Strøbæk, M. Skrzypczak, L. F. Andersson, S. Buus, A. S. Buus, J. P. Christensen, T. J. Dalebout, K. Iversen, L. H. Harritshøj, B. Mordmüller, H. Ullum, L. S. Reinert, W. A. de Jongh, M. Kikkert, S. R. Paludan, T. G. Theander, M. A. Nielsen, A. Salanti, A. F. Sander, Capsid-like particles decorated with the SARS-CoV-2 receptor-binding domain elicit strong virus neutralization activity. *Nat. Commun.* **12**, 324 (2021).
15. W. Tai, L. He, X. Zhang, J. Pu, D. Voronin, S. Jiang, Y. Zhou, L. Du, Characterization of the receptor-binding domain (RBD) of 2019 novel coronavirus: Implication for development of RBD protein as a viral attachment inhibitor and vaccine. *Cell. Mol. Immunol.* **17**, 613–620 (2020).
16. L. Piccoli, Y. J. Park, M. A. Tortorici, N. Czudnochowski, A. C. Walls, M. Beltramello, C. Silacci-Fregni, D. Pinto, L. E. Rosen, J. E. Bowen, O. J. Acton, S. Jaconi, B. Guarino, A. Minola, F. Zatta, N. Sprugasci, J. Bassi, A. Peter, A. De Marco, J. C. Nix, F. Mele, S. Jovic, B. F. Rodriguez, S. V. Gupta, F. Jin, G. Piumatti, G. Lo Presti, A. F. Pellanda, M. Biggiogero, M. Tarkowski, M. S. Pizzuto, E. Cameroni, C. Havenar-Daughton, M. Smithey, D. Hong, V. Lepori, E. Albanese, A. Ceschi, E. Bernasconi, L. Elzi, P. Ferrari, C. Garzoni, A. Riva, G. Snell, F. Sallusto, K. Fink, H. W. Virgin, A. Lanzavecchia, D. Corti, D. Veesler, Mapping neutralizing and immunodominant sites on the SARS-CoV-2 spike receptor-binding domain by structure-guided high-resolution serology. *Cell* **183**, 1024–1042.e21 (2020).
17. R. G. King, A. Silva-Sanchez, J. N. Peel, D. Botta, A. M. Dickson, A. K. Pinto, S. Meza-Perez, S. R. Allie, M. D. Schultz, M. Liu, J. E. Bradley, S. Qiu, G. Yang, F. Zhou, E. Zumaquero, T. S. Simpler, B. Mousseau, J. T. Killian, B. Dean, Q. Shang, J. L. Tipper, C. A. Risley, K. S. Harrod, T. Feng, Y. Lee, B. Shiberu, V. Krishnan, I. Peguillet, J. Zhang, T. J. Green, T. D. Randall, J. J. Suschak, B. Georges, J. D. Brien, F. E. Lund, M. S. Roberts, Single-dose intranasal administration of AdCOVID elicits systemic and mucosal immunity against SARS-CoV-2 and fully protects mice from lethal challenge. *Vaccine* **9**, 881 (2021).
18. N. C. Kyriakidis, A. Lopez-Cortes, E. V. Gonzalez, A. B. Grimaldos, E. O. Prado, SARS-CoV-2 vaccines strategies: A comprehensive review of phase 3 candidates. *NPJ Vaccines* **6**, 28 (2021).
19. N. Wang, J. Shang, S. Jiang, L. Du, Subunit vaccines against emerging pathogenic human coronaviruses. *Front. Microbiol.* **11**, 298 (2020).
20. H.-X. Tan, J. A. Juno, W. S. Lee, I. Barber-Axthelm, H. G. Kelly, K. M. Wragg, R. Esterbauer, T. Amarasena, F. L. Mordant, K. Subbarao, S. J. Kent, A. K. Wheatley, Immunogenicity of prime-boost protein subunit vaccine strategies against SARS-CoV-2 in mice and macaques. *Nat. Commun.* **12**, 1403 (2021).
21. R. J. Garten, C. T. Davis, C. A. Russell, B. Shu, S. Lindstrom, A. Balish, W. M. Sessions, X. Xu, E. Skepner, V. Deyde, M. Okomo-Adhiambo, L. Gubareva, J. Barnes, C. B. Smith, S. L. Emery, M. J. Hillman, P. Rivailler, J. Smagala, M. d. Graaf, D. F. Burke, R. A. M. Fouchier, C. Pappas, C. M. Alpuche-Aranda, H. López-Gatell, H. Olivera, I. López, C. A. Myers, D. Faix, P. J. Blair, C. Yu, K. M. Keene, P. D. Dotson, D. Boxrud, A. R. Sambol, S. H. Abid, K. S. George, T. Bannerman, A. L. Moore, D. J. Stringer, P. Blevins, G. J. Demmler-Harrison, M. Ginsberg, P. Kriner, S. Waterman, S. Smole, H. F. Guevara, E. A. Belongia, P. A. Clark, S. T. Beatrice, R. Donis, J. Katz, L. Finelli, C. B. Bridges, M. Shaw, D. B. Jernigan, T. M. Uyeki, D. J. Smith, A. I. Klimov, N. J. Cox, Antigenic and genetic characteristics of swine-origin 2009 A (H1N1) influenza viruses circulating in humans. *Science* **325**, 197–201 (2009).
22. J. Feng, U. Gulati, X. Zhang, W. A. Keitel, D. M. Thompson, J. A. James, L. F. Thompson, G. M. Air, Antibody quantity versus quality after influenza vaccination. *Vaccine* **27**, 6358–6362 (2009).
23. S. Ashkenazi, A. Vertruyen, J. Aristegui, S. Esposito, D. D. McKeith, T. Klemola, J. Biolek, J. Kuhr, T. Bujnowski, D. Desgrandchamps, S. M. Cheng, J. Skinner, W. C. Gruber, B. D. Forrest; CAIV-T Study Group, Superior relative efficacy of live attenuated influenza vaccine compared with inactivated influenza vaccine in young children with recurrent respiratory tract infections. *Pediatr. Infect. Dis. J.* **25**, 870–879 (2006).
24. J. Duffy, M. Lewis, T. Harrington, R. Baxter, E. A. Belongia, L. A. Jackson, S. J. Jacobsen, G. M. Lee, A. L. Naleway, J. Nordin, M. F. Daley; Vaccine Safety Datalink, Live attenuated influenza vaccine use and safety in children and adults with asthma. *Ann. Allergy Asthma Immunol.* **118**, 439–444 (2017).
25. M. Keshavarz, H. Mirzaei, M. Salemi, F. Momeni, M. J. Mousavi, M. Sadeghalvad, Y. Arjeini, F. Solaymani-Mohammadi, J. Sadri Nahand, H. Namdari, T. Mokhtari-Azad, F. Rezaei, Influenza vaccine: Where are we and where do we go? *Rev. Med. Virol.* **29**, e2014 (2019).
26. G. Fink, N. Orlova-Fink, T. Schindler, S. Grisi, A. P. Ferrer, C. Daubenberger, A. Brentani, Inactivated trivalent influenza vaccination is associated with lower mortality among patients with COVID-19 in Brazil. *BMJ Evid. Based Med.* **26**, 192–193 (2021).
27. Q. Gao, L. Bao, H. Mao, L. Wang, K. Xu, M. Yang, Y. Li, L. Zhu, N. Wang, Z. Lv, H. Gao, X. Ge, B. Kan, Y. Hu, J. Liu, F. Cai, D. Jiang, Y. Yin, C. Qin, J. Li, X. Gong, X. Lou, W. Shi, D. Wu, H. Zhang, L. Zhu, W. Deng, Y. Li, J. Lu, C. Li, X. Wang, W. Yin, Y. Zhang, C. Qin, Development of an inactivated vaccine candidate for SARS-CoV-2. *Science* **369**, 77–81 (2020).
28. A. L. St. John, C. Y. Chan, H. F. Staats, K. W. Leong, S. N. Abraham, Synthetic mast-cell granules as adjuvants to promote and polarize immunity in lymph nodes. *Nat. Mater.* **11**, 250–257 (2012).
29. C. Fu, T. Liu, L. Li, H. Liu, D. Chen, F. Tang, The absorption, distribution, excretion and toxicity of mesoporous silica nanoparticles in mice following different exposure routes. *Biomaterials* **34**, 2565–2575 (2013).
30. Y. Yahalom-Ronen, H. Tamir, S. Melamed, B. Politi, O. Shifman, H. Achdout, E. B. Vitner, O. Israeli, E. Milrot, D. Stein, I. Cohen-Gihon, S. Lazar, H. Gutman, I. Glinert, L. Cherry, Y. Vagima, S. Lazar, S. Weiss, A. Ben-Shmuel, R. Avraham, R. Puni, E. Lupu, E. Bar-David, A. Sittner, N. Erez, R. Zichel, E. Mamroud, O. Mazor, H. Levy, O. Laskar, S. Yitzhaki, S. C. Shapira, A. Zvi, A. Beth-Din, N. Paran, T. Israely, A single dose of recombinant VSV-ΔG-spike vaccine provides protection against SARS-CoV-2 challenge. *Nat. Commun.* **11**, 6402 (2020).
31. U. Sahin, A. Muik, I. Vogler, E. Derhovanessian, L. M. Kranz, M. Vormehr, J. Quandt, N. Bidmon, A. Ulges, A. Baum, K. E. Pascal, D. Maurus, S. Brachtendorf, V. Lorks, J. Sikorski, P. Koch, R. Hilker, D. Becker, A. K. Eller, J. Grutzner, M. Tonigold, C. Boesler, C. Rosenbaum, L. Heesen, M. C. Kuhnle, A. Poran, J. Z. Dong, U. Luxemburger, A. Kemmer-Bruck, D. Langer, M. Bexon, S. Bolte, T. Palanche, A. Schultz, S. Baumann, A. J. Mahiny, G. Boros, J. Reinholz, G. T. Szabo, K. Kariko, P. Y. Shi, C. Fontes-Garfias, J. L. Perez, M. Cutler, D. Cooper, C. A. Kyratsous, P. R. Dormitzer, K. U. Jansen, O. Tureci, BNT162b2 vaccine induces neutralizing antibodies and poly-specific T cells in humans. *Nature* **595**, 572–577 (2021).
32. A. B. Vogel, I. Kanevsky, Y. Che, K. A. Swanson, A. Muik, M. Vormehr, L. M. Kranz, K. C. Walzer, S. Hein, A. Güler, J. Loschko, M. S. Maddur, A. Ota-Setlik, K. Tompkins, J. Cole, B. G. Lui, T. Ziegenhals, A. Plaschke, D. Eisel, S. C. Dany, S. Fesser, S. Erbar, F. Bates, D. Schneider, B. Jesionek, B. Sänger, A. K. Wallisch, Y. Feuchter, H. Junginger, S. A. Krumm, A. P. Heinen, P. Adams-Quack, J. Schlereth, S. Schille, C. Kroner, R. de la Caridad Güimil Garcia, T. Hiller, L. Fischer, R. S. Sellers, S. Choudhary, O. Gonzalez, F. Vascotto, M. R. Gutman, J. A. Fontenot, S. Hall-Ursone, K. Brasky, M. C. Griffor, S. Han, A. A. H. Su, J. A. Lees, N. L. Nedoma, E. H. Mashalidis, P. V. Sahasrabudhe, C. Y. Tan, D. Pavliakova, G. Singh, C. Fontes-Garfias, M. Pride, I. L. Scully, T. Ciolino, J. Obregon, M. Gazi, R. Carrion Jr., K. J. Alfson, W. V. Kalina, D. Kaushal, P.-Y. Shi, T. Klamp, C. Rosenbaum, A. N. Kuhn, Ö. Türeci, P. R. Dormitzer, K. U. Jansen, U. Sahin, BNT162b vaccines protect rhesus macaques from SARS-CoV-2. *Nature* **592**, 283–289 (2021).
33. M. A. Maier, M. Jayaraman, S. Matsuda, J. Liu, S. Barros, W. Querbes, Y. K. Tam, S. M. Ansell, V. Kumar, J. Qin, X. Zhang, Q. Wang, S. Panesar, R. Hutabarat, M. Carioto, J. Hettinger, P. Kandasamy, D. Butler, K. G. Rajeev, B. Pang, K. Charisse, K. Fitzgerald, B. L. Mui, X. Du, P. Cullis, T. D. Madden, M. J. Hope, M. Manoharan, A. Akinc, Biodegradable lipids enabling rapidly eliminated lipid nanoparticles for systemic delivery of RNAi therapeutics. *Mol. Ther.* **21**, 1570–1578 (2013).
34. Pfizer-BioNTech COVID-19 Vaccine—Fact Sheet for Healthcare Providers Administering Vaccine (FDA, accessed 15 April 2021); www.fda.gov/media/167211/download.
35. J. Zepeda-Cervantes, J. O. Ramirez-Jarquin, L. Vaca, Interaction between virus-like particles (VLPs) and pattern recognition receptors (PRRs) from dendritic cells (DCs): Toward better engineering of VLPs. *Front. Immunol.* **11**, 1100 (2020).
36. T. Korn, E. Bettelli, M. Oukka, V. K. Kuchroo, IL-17 and Th17 cells. *Annu. Rev. Immunol.* **27**, 485–517 (2009).

37. S. F. Sia, L.-M. Yan, A. W. H. Chin, K. Fung, K.-T. Choy, A. Y. L. Wong, P. Kaewpreedee, R. Perera, L. L. M. Poon, J. M. Nicholls, M. Peiris, H.-L. Yen, Pathogenesis and transmission of SARS-CoV-2 in golden Syrian hamsters. *Nature* **583**, 834–838 (2020).
38. L. H. Tostanoski, F. Wegmann, A. J. Martinot, C. Loos, K. McMahan, N. B. Mercado, J. Yu, C. N. Chan, S. Bondoc, C. E. Starke, M. Nekorchuk, K. Busman-Sahay, C. Piedra-Mora, L. M. Wrijil, S. Ducat, J. Custers, C. Atyeo, S. Fischinger, J. S. Burke, J. Feldman, B. M. Hauser, T. M. Caradonna, E. A. Bondzie, G. Dagotto, M. S. Gebre, C. Jacob-Dolan, Z. Lin, S. H. Mahrokhian, F. Nampanya, R. Nityanandam, L. Pessaint, M. Porto, V. Ali, D. Benetiene, K. Tevi, H. Andersen, M. G. Lewis, A. G. Schmidt, D. A. Lauffenburger, G. Alter, J. D. Estes, H. Schuitemaker, R. Zahn, D. H. Barouch, Ad26 vaccine protects against SARS-CoV-2 severe clinical disease in hamsters. *Nat. Med.* **26**, 1694–1700 (2020).
39. Y. J. Hou, S. Chiba, P. Halfmann, C. Ehre, M. Kuroda, K. H. Dinnon III, S. R. Leist, A. Schafer, N. Nakajima, K. Takahashi, R. E. Lee, T. M. Mascenik, R. Graham, C. E. Edwards, L. V. Tse, K. Okuda, A. J. Markmann, L. Bartelt, A. de Silva, D. M. Margolis, R. C. Boucher, S. H. Randell, T. Suzuki, L. E. Gralinski, Y. Kawaoka, R. S. Baric, SARS-CoV-2 D614G variant exhibits efficient replication ex vivo and transmission in vivo. *Science* **370**, 1464–1468 (2020).
40. A. Chandrashekar, J. Liu, A. J. Martinot, K. McMahan, N. B. Mercado, L. Peter, L. H. Tostanoski, J. Yu, Z. Maliga, M. Nekorchuk, K. Busman-Sahay, M. Terry, L. M. Wrijil, S. Ducat, D. R. Martinez, C. Atyeo, S. Fischinger, J. S. Burke, M. D. Slein, L. Pessaint, A. Van Ry, J. Greenhouse, T. Taylor, K. Blade, A. Cook, B. Finneyfrock, R. Brown, E. Teow, J. Velasco, R. Zahn, F. Wegmann, P. Abbink, E. A. Bondzie, G. Dagotto, M. S. Gebre, X. He, C. Jacob-Dolan, N. Kordana, Z. Li, M. A. Lifton, S. H. Mahrokhian, L. F. Maxfield, R. Nityanandam, J. P. Nkolola, A. G. Schmidt, A. D. Miller, R. S. Baric, G. Alter, P. K. Sorger, J. D. Estes, H. Andersen, M. G. Lewis, D. H. Barouch, SARS-CoV-2 infection protects against rechallenge in rhesus macaques. *Science* **369**, 812–817 (2020).
41. M. Aid, K. Busman-Sahay, S. J. Vidal, Z. Maliga, S. Bondoc, C. Starke, M. Terry, C. A. Jacobson, L. Wrijil, S. Ducat, O. R. Brook, A. D. Miller, M. Porto, K. L. Pellegrini, M. Pino, T. N. Hoang, A. Chandrashekar, S. Patel, K. Stephenson, S. E. Bosinger, H. Andersen, M. G. Lewis, J. L. Hecht, P. K. Sorger, A. J. Martinot, J. D. Estes, D. H. Barouch, Vascular disease and thrombosis in SARS-CoV-2-infected rhesus macaques. *Cell* **183**, 1354–1366.e13 (2020).
42. P. Mlcochova, S. A. Kemp, M. S. Dhar, G. Papa, B. Meng, I. Ferreira, R. Datir, D. A. Collier, A. Albecka, S. Singh, R. Pandey, J. Brown, J. Zhou, N. Goonawardane, S. Mishra, C. Whittaker, T. Mellan, R. Marwal, M. Datta, S. Sengupta, K. Ponnusamy, V. S. Radhakrishnan, A. Abdullahi, O. Charles, P. Chattopadhyay, P. Devi, D. Caputo, T. Peacock, C. Wattal, N. Goel, A. Satwik, R. Vaishya, M. Agarwal; The indian SARS-CoV-2 Genomics Consortium (INSACOG); The Genotype to Phenotype Japan (G2P-Japan) Consortium; The CITIID-NIHR BioResource COVID-19 Collaboration, A. Mavousian, J. H. Lee, J. Bassi, C. Silacci-Fegni, C. Saliba, D. Pinto, T. Irie, I. Yoshida, W. L. Hamilton, K. Sato, S. Bhatt, S. Flaxman, L. C. James, D. Corti, L. Piccoli, W. S. Barclay, P. Rakshit, A. Agrawal, R. K. Gupta, SARS-CoV-2 B.1.617.2 Delta variant replication and immune evasion. *Nature* **599**, 114–119 (2021).
43. K. B. Pouwels, E. Pritchard, P. C. Matthews, N. Stoesser, D. W. Eyre, K. D. Vihta, T. House, J. Hay, J. I. Bell, J. N. Newton, J. Farrar, D. Crook, D. Cook, E. Rourke, R. Studley, T. E. A. Peto, I. Diamond, A. S. Walker, Effect of Delta variant on viral burden and vaccine effectiveness against new SARS-CoV-2 infections in the UK. *Nat. Med.* **27**, 2127–2135 (2021).
44. A. Saito, T. Irie, R. Suzuki, T. Maemura, H. Nasser, K. Uriu, Y. Kosugi, K. Shirakawa, K. Sadamasu, I. Kimura, J. Ito, J. Wu, K. Iwatsuki-Horimoto, M. Ito, S. Yamayoshi, S. Loeber, M. Tsuda, L. Wang, S. Ozono, E. P. Butlertanaka, Y. L. Tanaka, R. Shimizu, K. Shimizu, K. Yoshimatsu, R. Kawabata, T. Sakaguchi, K. Tokunaga, I. Yoshida, H. Asakura, M. Nagashima, Y. Kazuma, R. Nomura, Y. Horisawa, K. Yoshimura, A. Takaori-Kondo, M. Imai; The Genotype to Phenotype Japan (G2P-Japan) Consortium, S. Tanaka, S. Nakagawa, T. Ikeda, T. Fukuhara, Y. Kawaoka, K. Sato, Enhanced fusogenicity and pathogenicity of SARS-CoV-2 Delta P681R mutation. *Nature* **602**, 300–306 (2022).
45. Z. Li, Z. Wang, P. C. Dinh, D. Zhu, K. D. Popowski, H. Lutz, S. Hu, M. G. Lewis, A. Cook, H. Andersen, J. Greenhouse, L. Pessaint, L. J. Lobo, K. Cheng, Cell-mimicking nanodecoys neutralize SARS-CoV-2 and mitigate lung injury in a non-human primate model of COVID-19. *Nat. Nanotechnol.* **16**, 942–951 (2021).
46. X. Zhou, X. Jiang, M. Qu, G. E. Aninwene, V. Jucaud, J. J. Moon, Z. Gu, W. Sun, A. Khademhosseini, Engineering antiviral vaccines. *ACS Nano* **14**, 12370–12389 (2020).
47. A. Muik, A.-K. Wallisch, B. Sänger, K. A. Swanson, J. Mühl, W. Chen, H. Cai, D. Maurus, R. Sarkar, Ö. Türeci, P. R. Dormitzer, U. Şahin, Neutralization of SARS-CoV-2 lineage B.1.1.7 pseudovirus by BNT162b2 vaccine–Elicited human sera. *Science* **371**, 1152–1153 (2021).
48. D. Laczko, M. J. Hogan, S. A. Toulmin, P. Hicks, K. Lederer, B. T. Gaudette, D. Castano, F. Amanat, H. Muramatsu, T. H. Oguin III, A. Ojha, L. Zhang, Z. Mu, R. Parks, T. B. Manzoni, B. Roper, S. Strohmeier, I. Tombacz, L. Arwood, R. Nachbagauer, K. Kariko, J. Greenhouse, L. Pessaint, M. Porto, T. Putman-Taylor, A. Strasbaugh, T. A. Campbell, P. J. C. Lin, Y. K. Tam, G. D. Sempowski, M. Farzan, H. Choe, K. O. Saunders, B. F. Haynes, H. Andersen, L. C. Eisenlohr, D. Weissman, F. Krammer, P. Bates, D. Allman, M. Locci, N. Pardi, A single immunization with nucleoside-modified mRNA vaccines elicits strong cellular and humoral immune responses against SARS-CoV-2 in mice. *Immunity* **53**, 724–732.e7 (2020).
49. Q. Ding, P. Lu, Y. Fan, Y. Xia, M. Liu, The clinical characteristics of pneumonia patients coinfected with 2019 novel coronavirus and influenza virus in Wuhan, China. *J. Med. Virol.* **92**, 1549–1555 (2020).
50. E. Tayar, S. Abdeen, M. A. Alah, H. Chemaitelly, I. Bougmiza, H. H. Ayoub, A. H. Kaleeckal, A. N. Latif, R. M. Shaik, H. E. Al-Romaihi, M. H. Al-Thani, R. Bertollini, L. J. Abu-Raddad, A. Al-Khal, Effectiveness of influenza vaccination against SARS-CoV-2 infection among healthcare workers in Qatar. *J. Infect. Public Health* **16**, 250–256 (2023).
51. L. He, X. Lin, Y. Wang, C. Abraham, C. Sou, T. Ngo, Y. Zhang, I. A. Wilson, J. Zhu, Single-component, self-assembling, protein nanoparticles presenting the receptor binding domain and stabilized spike as SARS-CoV-2 vaccine candidates. *Sci. Adv.* **7**, eabf1591 (2021).
52. J. G. Donahue, B. A. Kieke, J. P. King, M. A. Mascola, T. T. Shimabukuro, F. DeStefano, K. E. Hanson, D. L. McClure, O. Olaiya, J. M. Glanz, R. C. Hechter, S. A. Irving, L. A. Jackson, N. P. Klein, A. L. Naleway, E. S. Weintraub, E. A. Belongia, Inactivated influenza vaccine and spontaneous abortion in the Vaccine Safety Datalink in 2012-13, 2013-14, and 2014-15. *Vaccine* **37**, 6673–6681 (2019).
53. S. Toback, E. Galiza, C. Cosgrove, J. Galloway, A. L. Goodman, P. A. Swift, S. Rajaram, A. Graves-Jones, J. Edelman, F. Burns, A. M. Minassian, I. Cho, L. Kumar, J. S. Plested, E. J. Rivers, A. Robertson, F. Dubovsky, G. Glenn, P. T. Heath; 2019nCoV-302 Study Group, Safety, immunogenicity, and efficacy of a COVID-19 vaccine (NVX-CoV2373) co-administered with seasonal influenza vaccines: An exploratory substudy of a randomised, observer-blinded, placebo-controlled, phase 3 trial. *Lancet Respir. Med.* **10**, 167–179 (2022).
54. R. Lazarus, S. Baos, H. Cappel-Porter, A. Carson-Stevens, M. Clout, L. Culliford, S. R. Emmett, J. Garstang, L. Gbadamoshi, B. Hallis, R. A. Harris, D. Hutton, N. Jacobsen, K. Joyce, R. Kaminski, V. Libri, A. Middleditch, L. McCullagh, E. Moran, A. Phillipson, E. Price, J. Ryan, R. Thirard, R. Todd, M. D. Snape, D. Tucker, R. L. Williams, J. S. Nguyen-Van-Tam, A. Finn, C. A. Rogers; ComfluCOV Trial Group, Safety and immunogenicity of concomitant administration of COVID-19 vaccines (ChAdOx1 or BNT162b2) with seasonal influenza vaccines in adults in the UK (ComFluCOV): A multicentre, randomised, controlled, phase 4 trial. *Lancet* **398**, 2277–2287 (2021).
55. R. Izikson, D. Brune, J.-S. Bolduc, P. Bourron, M. Fournier, T. M. Moore, A. Pandey, L. Perez, N. Sater, A. Shrestha, S. Wague, S. I. Samson, Safety and immunogenicity of a high-dose quadrivalent influenza vaccine administered concomitantly with a third dose of the mRNA-1273 SARS-CoV-2 vaccine in adults aged ≥65 years: A phase 2, randomised, open-label study. *Lancet Respir. Med.* **10**, 392–402 (2022).
56. K. D. Popowski, A. Moatti, G. Scull, D. Silkstone, H. Lutz, B. Lopez de Juan Abad, A. George, E. Belcher, D. Zhu, X. Mei, X. Cheng, M. Cislo, A. Ghodsi, Y. Cai, K. Huang, J. Li, A. C. Brown, A. Greenbaum, P. C. Dinh, K. Cheng, Inhalable dry powder mRNA vaccines based on extracellular vesicles. *Matter* **5**, 2960–2974 (2022).
57. K. L. Miranda, E. M. Dorneles, R. B. Pauletti, F. P. Poester, A. P. Lage, Brucella abortus S19 and RB51 vaccine immunogenicity test: Evaluation of three mice (BALB/c, Swiss and CD-1) and two challenge strains (544 and 2308). *Vaccine* **33**, 507–511 (2015).
58. J. H. Hurst, S. M. Heston, H. N. Chambers, H. M. Cunningham, M. J. Price, L. Suarez, C. G. Crew, S. Bose, J. N. Aquino, S. T. Carr, S. M. Griffin, S. H. Smith, K. Jenkins, T. S. Pfeiffer, J. Rodriguez, C. T. DeMarco, N. A. De Naeyer, T. C. Gurley, R. Louzao, C. Zhao, C. K. Cunningham, W. J. Steinbach, T. N. Denny, D. J. Lugo, M. A. Moody, S. R. Permar, A. T. Rotta, N. A. Turner, E. B. Walter, C. W. Woods, M. S. Kelly, Severe acute respiratory syndrome coronavirus 2 infections among children in the biospecimens from respiratory virus-exposed kids (BRAVE Kids) study. *Clin. Infect. Dis.* **73**, e2875–e2882 (2021).

Acknowledgments: We thank S. Kar, M. Porto, M. Lok, and B. Spence at BIOQUAL Inc. for performing the hamster studies. We thank N. De Naeyer, C. T. DeMarco, and T. N. Denny at Duke Human Vaccine Institute for performing viral load assay. We are indebted to J. Chung for synthesis of spike mRNA. **Funding:** This work was supported by grants from the National Institutes of Health (HL123920, HL144002, HL146153, HL147357, HL149940, and HL154154 to K.C.; HL164998 to P.C.D) and the American Heart Association (19EIA34660286 to K.C.). **Author contributions:** K.C., Z.W., and Z.L. conceived the idea. Z.W., K.C., and Z.L. designed the overall experiments. Z.W., Z.L., W.S., and D.Z. performed the experiments. Z.W. and K.C. wrote the article. W.S., S.H., and P.-U.C.D. reviewed and edited the article. K.C. supervised this research. All authors read and approved the final article. All authors provided the corresponding author with written permission to be named in the article. **Competing interests:** The authors declare that they have no competing interests. **Data and materials availability:** All data needed to evaluate the conclusions in the paper are present in the paper and/or the Supplementary Materials.

Submitted 1 February 2022
Accepted 19 May 2023
Published 23 June 2023
10.1126/sciadv.abo4100